

## Review

## Review of droplet entrainment in annular flow: Interfacial waves and onset of entrainment

C. Berna <sup>a,\*</sup>, A. Escrivá <sup>a</sup>, J.L. Muñoz-Cobo <sup>a</sup>, L.E. Herranz <sup>b,1</sup><sup>a</sup> Instituto de Ingeniería Energética, Universitat Politècnica de València (UPV), Camino de Vera 14, 46022 Valencia, Spain<sup>b</sup> Unit of Nuclear Safety Research, Division of Nuclear Fission, CIEMAT, Avda.Complutense 22, 28040 Madrid, Spain

## ARTICLE INFO

## Article history:

Received 13 September 2013

Received in revised form

17 December 2013

Accepted 29 January 2014

## Keywords:

Annular flow

Onset of entrainment

Gas–liquid interface

Film thickness

Wave celerity

Wave frequency

## ABSTRACT

Annular two-phase flow has been vastly investigated because of its large and deep involvement in industrial processes, particularly in nuclear engineering. This paper reviews most of the recent literature on the matter, with emphasis in all those variables and processes occurring in the liquid–gas interface that cause droplet entrainment. Further than presenting correlations, the paper shows the existing scattering found when expressions are compared to each other and it highlights the gaps of knowledge still existing. Additionally, based on some of the open data, alternate equations are derived for key variables in the annular flow descriptions, like liquid film thickness and wave celerity and frequency.

© 2014 Elsevier Ltd. All rights reserved.

## 1. Introduction

Two-phase gas–liquid flows are widely encountered in many different industrial applications: petroleum, chemical, civil and nuclear industries, and particularly in boiling and condensing heat transfer equipment. Nuclear power plants involve two-phase flow. In pressurized water reactors (PWRs) two-phase flow is especially encountered in the steam generators and in the upper-core components during normal operation and in the reactor itself during off-normal conditions, including accident sequences. In boiling water reactors (BWRs) the two-phase flow occurs in the core during normal operation. In all these processes two-phase flows play an important role in their operation, safety and cost that is why, a proper understanding of their behavior is particularly interesting. Consequently, a large number of publications have been performed focusing on the study of multiphase flow research, in particular its investigation began in the 40s and continues until present time.

Two-phase flows in pipes can be grouped into classes, commonly called flow regimes or flow patterns. The wide varieties of classifications that exist in the literature are mainly due to the

subjective nature of the characterization method, and as a general reference maps for vertical and horizontal flow are presented in Fig. 1.

In particular, the annular flow pattern can be found in many important industrial applications. For instance, in the evaporators and condensers of conventional power generating plants; in pressurized water reactors of nuclear power plants during a LOCA (loss of coolant accident) and in boiling water reactors during normal operation; in geothermal and gas-oil wells, etcetera. As a result, the ability to understand and model annular two-phase flow is a subject of central importance to achieve a reliable design of this equipment.

Annular flow is normally characterized by: a gas core flowing through the center of the tube; a part of the liquid, as a thin film, flowing on the tube wall; while the other part flows as entrained liquid droplets in the gas core. For horizontal pipes, at the beginning of the transition from stratified wavy to annular flow, only the gas core (without entrained droplets) and the thin liquid film exist. As the difference in velocity between gas and liquid phases increases, a series of waves begin to appear on the gas–liquid interface. When this difference is high enough, a flow rate of droplets is entrained from the liquid film surface into the core of the gas stream. The point in which this entrainment phenomenon starts is called “onset of entrainment” and its associated velocity is the entrainment inception velocity. These entrained droplets

\* Corresponding author. Tel.: +34 963879245.

E-mail addresses: [ceberes@upv.es](mailto:ceberes@upv.es) (C. Berna), [aescriva@iqn.upv.es](mailto:aescriva@iqn.upv.es) (A. Escrivá), [jlcobos@iqn.upv.es](mailto:jlcobos@iqn.upv.es) (J.L. Muñoz-Cobo), [luisen.herranz@ciemates.es](mailto:luisen.herranz@ciemates.es) (L.E. Herranz).

1 Tel.: +34 913466219; fax: +34 913466233.

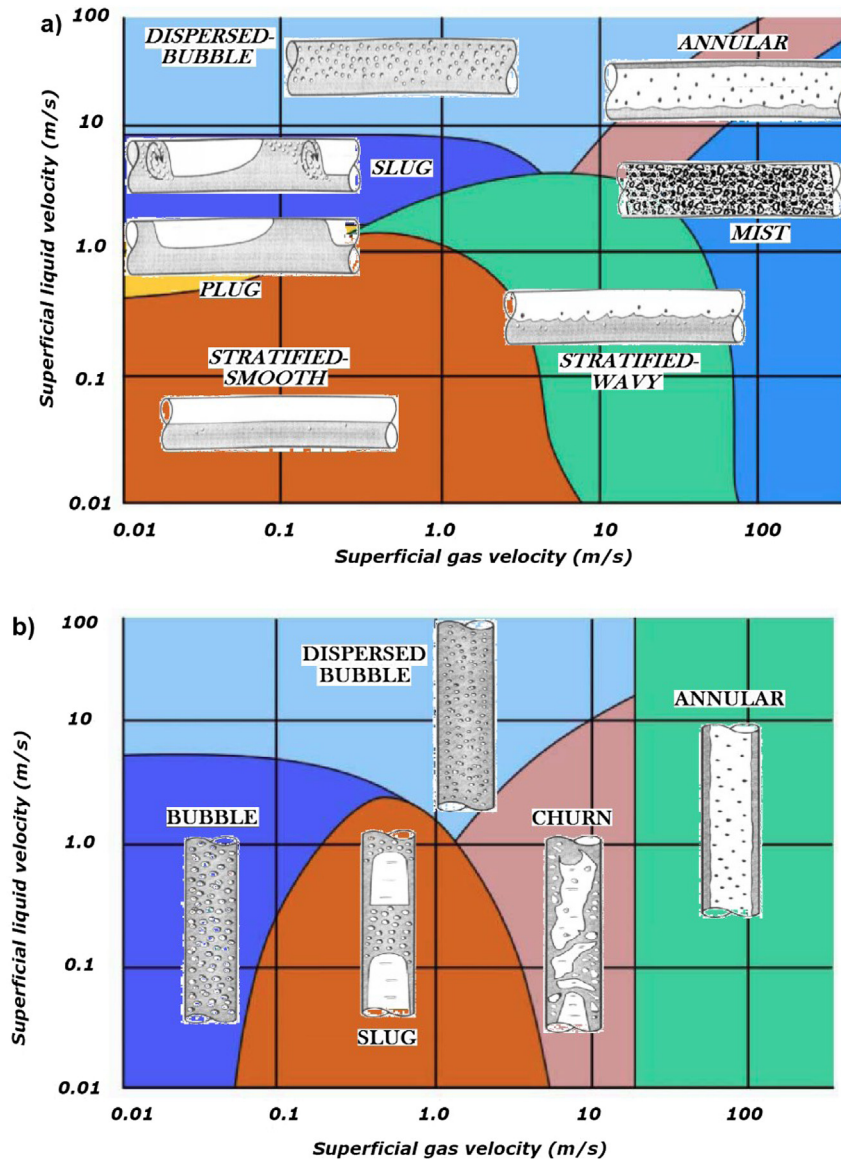


Fig. 1. Flow maps for two-phase gas–liquid flow: (a) vertical pipes; and (b) horizontal pipes.

contribute significantly to heat and mass transfer, and the modeling of the gas–liquid interface properties, droplets extraction mechanisms and droplets itself are of high practical interest. The contact area between the liquid film and the gas, gas–liquid interface, is covered with waves, and the water droplets are extracted from the crest of these waves and are then transported into the gas core by the high velocity gas stream.

This review presents and analyzes most of the extensive literature that exists on annular two-phase flow. In particular, the paper focuses on the study of the liquid film layer and the gas–liquid interface, presenting its main characteristics and analyzing the process of droplet extraction from this liquid phase to the gas phase (the entrainment process). The aim of this article is, firstly, to reveal the dispersion in the abundant information available, collecting them insofar as possible and, moreover, presenting the lacks of knowledge that still exist in annular flow. Secondly, its interest is to have on hand in the same document a summary of the various expressions found in the literature. And finally, several

analyses of the different experimental values found in the open literature have been made, presenting a new set of correlations for its adjustment.

In this work, we will focus on the study of the liquid film properties, gas–liquid interface and the mechanisms governing these water droplets extraction processes. To do so, this paper is organized as follows.

- First, in Section 2, we present a summary of the main characteristics of the waves that are present on the gas–liquid interface.
- Section 3 is devoted to present the onset of entrainment process.
- Section 4 focuses on the entrainment inception velocity.
- Section 5, in which the comparison of the experimental measurements, the results obtained with the different expressions available in the literature and the developed in the present work are presented.
- Finally, Section 6 settles the main conclusions from this study.

## 2. Waves on the annular flow

### 2.1. General description

It is generally assumed that two different types of waves can exist on the liquid film surface: long-length disturbance waves (DW), with amplitude several times higher than the average liquid film thickness, and small-scaled ripple waves (RW), Fig. 2. Then, for the physical modeling of the entrainment phenomenon, detailed information on the origin of these two types of waves is needed. Respect to RW, they are considered to be omnipresent on the film surface in the presence of a turbulent gas stream, even for very low liquid film Reynolds numbers. Regarding the DW, they appear when the liquid flow rate grows, and, consequently, the entrainment occurs.

Hundreds of interfacial wave behavior studies have been carried out by different authors in both vertical and horizontal flows. All of them refer to the existence of two types of waves, the first one have small amplitudes compared with the liquid film thickness, move at low velocities, their lifetime is short, they usually do not occupy the whole tube circumference and do not appear to carry mass (Hewitt and Govan, 1990; Schubring and Shedd, 2008; Alekseenko et al., 2008, 2009). The second type of waves have a longer lifespan, their amplitudes are usually several times the liquid film thickness and carry mass along the tube (Hanratty and Hersman, 1961; Asali and Hanratty, 1993; Schubring and Shedd, 2008; Alekseenko et al., 2008, 2009). For vertical tubes, in the order of 6 cm or smaller, the liquid film is uniformly distributed around the tube circumference (Asali et al., 1985), and the disturbance waves appear circumferentially coherent (Hall-Taylor et al., 1963; Hewitt and Lovegrove, 1969; Asali and Hanratty, 1993) and symmetrical (Hewitt and Hall-Taylor, 1970; Ohba and Nagae, 1993). The work made by Martin (1983) shows that waves are highly regular in tubes with an inner diameter of 1 cm. The disturbance waves present a long region of relatively quiet fluid between crests (Wallis, 1969). Sekoguchi et al. (1985) presented images of disturbance waves, which were directly based on their measurements in vertical annular flow in a 25.8-mm tube. Zhu's (2004) physical wave model provides similar wave profiles based on the measurement data of MacGillivray (2004) in vertical annular flow in a 9.525 mm tube. An important aspect to emphasize is the fact that, in vertical annular flow, all its properties tend to be distributed uniformly around the pipe circumference. But in the case of horizontal annular flow, there is a highly asymmetric distribution of all its properties due to the gravity force. For instance, as it is shown by the work in horizontal flow conditions of Paras and Karabelas (1991) for low gas flow rates (gas velocities lower than 40–50 m/s approximately) and for all

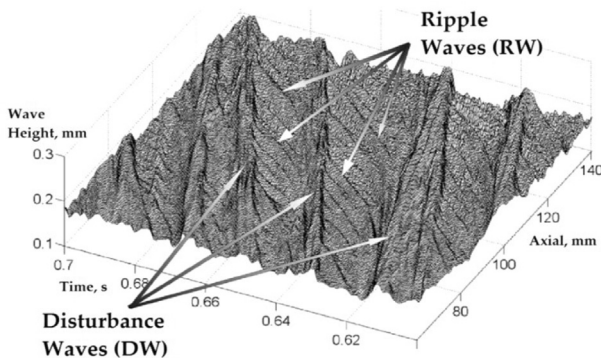


**Fig. 2.** Three-dimensional representation of wave height, axial component and time evolution in the entrainment regime.

liquid rates tested, all the film properties are highly asymmetric; but as the gas flow rate increases, all its properties tend to be distributed uniformly around the pipe circumference. This implies that the role of gravity is almost negligible at high velocities, the values of film properties at the top of the pipe are almost 80% of the ones at the bottom for gas velocities of 50 m/s.

At very low liquid flow rates the ripple waves dominate the two-phase interface. Above a critical liquid flow rate, disturbance waves appear in the flow (Andreussi et al., 1985; Schadel, 1988), where they exert a strong influence due to their significant dimensions and dynamic properties. Although both types of waves exist over the full range of annular flow, due to the minor role of the last ones, only the disturbance waves are studied here.

As it has been explained earlier, when the liquid mass flow rate is above its critical value the disturbance waves are the ones prevailing, in this case, several transitions can take place depending on the gas velocity (Hewitt and Hall-Taylor, 1970; Wallis, 1969; Brodkey, 1967; Van Rossum, 1959; Lamb, 1975; Levich, 1962). When the gas velocity is very small, the interface presents a relative stability. However, with the increase in the gas velocity, it can be said that the interface becomes wavy due to the well-known Kelvin-Helmholtz instability (Lamb, 1975; Levich, 1962). In horizontal and inclined pipes or channels, the gravity and surface tension force has a stabilizing effect, whereas the relative velocity between the phases destabilizes the film by variation in pressure distribution over the wave. At the wave crest, the gas velocity is higher, corresponding to a lower pressure, according to the Bernoulli theorem, and through the wave trough there is a lower gas velocity which results in a higher gas pressure. When the relative velocity between the gas and the liquid film is further increased, the waves become irregular and three-dimensional (Van Rossum, 1959; Hanratty and Hersman, 1961). These are the roll waves studied by Hanratty and Engen (1957), Hanratty and Hersman (1961), Chung and Murgatroyd (1965), Brodkey (1967), Wallis (1969), etc. Detailed experimental works using various liquids were carried out by Van Rossum (1959), whose data indicate that there exist several different mechanisms of entrainment, not only the above mentioned roll wave mechanism. As a consequence, the next step will be to describe these waves.

### 2.2. Wave characteristics

An adequate characterization of the waves in the gas–liquid interface is important for entrainment modeling, because wave

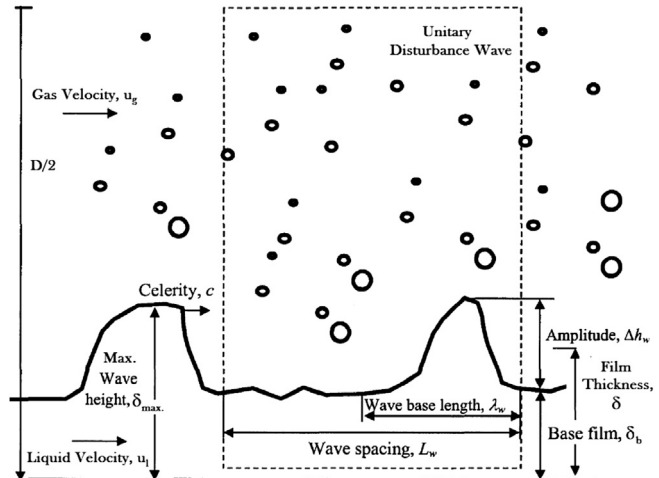


**Fig. 3.** Schematic view of an unit disturbance wave.

modeling deals with the prediction of the conditions at which waves are formed and become unstable. A complete description of their characteristics involves obtaining: celerity, wavelength, amplitude and shape, etcetera, see Fig 3.

Referring to Fig. 3, the following terms are of significance in the characterization of the disturbance wave shape. The wave spacing,  $L_w$ , is equal to the total measured length of the film time trace divided by the number of peaks that appear in this entire time trace. The wave peak height or maximum wave height,  $\delta_{\max}$ , is obtained as the average of the observed peaks in the film time trace. The base film thickness or wave base height,  $\delta_b$ , is defined as the average value of the film thickness between the ending point of a wave and the starting point of the next one. The wave amplitude or wave roughness height,  $\Delta h_w$ , is defined as the difference between the wave peak height and the wave base height. Celerity,  $c$ , is the wave displacement velocity. The wave base length or wave width,  $\lambda_w$ , is the distance between the starting point and ending point of a single wave. Another definition that is not shown in the figure is the wave separation, which is defined as the distance between the starting point of one wave and the ending point of the previous one, it also corresponds to the wave spacing minus wave base length.

### 2.2.1. Liquid film thickness

Liquid film thickness is the distance from the pipe wall to a mean height of the waves produced into the gas–liquid interface, see Fig. 3.

**2.2.1.1. Ambrosini's correlation** (Fukano and Furukawa, 1998; Rodriguez, 2009). Kosky was one of the first authors to develop a model to obtain the liquid film thickness for vertical upward flows. He performed a balance force for the liquid film assuming the velocity profile to be that for single phase turbulent flow. Since the turbulent profile used depended on the height of the film, Kosky derived the following two equations for the dimensionless film thickness

$$\delta_l^+ = \sqrt{2} Re_{lf}^{0.5} \quad (1)$$

for  $\delta_l^+ < 25$  (low  $Re_{lf}$ ), whereas for  $\delta_l^+ > 25$  (high  $Re_{lf}$ ) recommends the next relationship

$$\delta_l^+ = 0.0512 Re_{lf}^{0.875} \quad (2)$$

being  $Re_{lf}$  the liquid film Reynolds number defines as

$$Re_{lf} = \frac{4W_{lf}}{\mu_l P} = \frac{4\Gamma_{lf}}{\mu_l} = \frac{4\rho_l u_{lf} \delta}{\mu_l} \quad (3)$$

where  $W_{lf}$  is the mass flow rate of the liquid in the wall layer;  $P$  is the wetted perimeter of the pipe or channel;  $\Gamma_{lf}$  is the mass flow rate of the liquid film per circumferential length unit.

The dimensionless thickness is defined as

$$\delta_l^+ = \frac{\rho_l \delta u_l^*}{\mu_l} \quad (4)$$

where  $u_l^*$  is the friction velocity, which is expressed as

$$u_l^* = \sqrt{\frac{\tau_c}{\rho_l}} \quad (5)$$

where  $\tau_c$  is a characteristic shear stress, and approximately equal to the interfacial shear stress,  $\tau_i$ , being defined as

$$\tau_i = \frac{1}{2} f_{gi} \rho_g (u_g - u_{lf})^2 \quad (6)$$

where  $f_{gi}$  is the interfacial friction factor, one of the most popular expressions to calculate this friction factor is the Wallis correlation,

$$f_{gi} = 0.005 \left( 1 + 300 \frac{\delta}{D} \right) \quad (7)$$

This correlation has been modified over the years, and lots of different correlations are available in the open literature, but the most widely used is

$$f_{gi} = f_g \left( 1 + 300 \frac{\delta}{D} \right) \quad (8)$$

where  $f_g$  is the single-phase gas friction factor, usually defined as

$$f_g = \frac{0.079}{Re_g^{0.25}} \quad (9)$$

Regarding the gas and liquid superficial velocities, say that they are related with the expressions of the gas and liquid velocities, since the liquid film is thin and almost all the pipe is occupied by the gas phase, then

$$\begin{aligned} u_g &\approx J_g \\ u_{lf} &\approx \frac{D}{4\delta} J_{lf} \end{aligned} \quad (10)$$

Asali, from his data for low  $Re_{lf}$  ( $Re_{lf} \approx 20$ –300), proposed a modification of the Kosky expression to low  $Re_{lf}$ . He recommended the following expression

$$\delta_l^+ = 0.34 Re_{lf}^{0.6} \quad (11)$$

Several years later, Ambrosini re-correlated the previously developed expressions with a wide range of data, in which pipe diameters and working fluids had been varied. They found that the data were best fitted using the mean film thickness correlation of Asali for  $Re_{lf} < 1000$ , Eq. (11), and the high  $Re_{lf}$  model of Kosky for  $Re_{lf} > 1000$ , Eq. (2)

$$\delta_l^+ = \frac{\rho_l \delta u_l^*}{\mu_l} = \begin{cases} 0.34 Re_{lf}^{0.6} & Re_{lf} \leq 1000 \\ 0.0512 Re_{lf}^{0.875} & Re_{lf} > 1000 \end{cases} \quad (12)$$

**2.2.1.2. Fukano's correlation** (Fukano and Furukawa, 1998). Another expression to estimate the liquid film thickness for vertical upward flows proposed by Fukano is

$$\frac{\delta}{D} = 0.0594 \exp \left( -0.34 Fr_g^{0.25} Re_l^{0.19} x^{0.6} \right) \quad (13)$$

where  $Fr_g$  is the gas Froude number defined by the superficial velocity of the gas phase,  $Re_l$  is the liquid film Reynolds number defined by the superficial velocity of the liquid phase and  $x^*$  is the gas quality. These magnitudes are defined as follows

$$Fr_g = \frac{J_g}{\sqrt{gD}} \quad (14)$$

$$Re_l = \frac{\rho_l J_l D}{\mu_l} \quad (15)$$

$$x^* = \frac{J_g \rho_g}{J_g \rho_g + J_l \rho_l} \quad (16)$$

Since part of the total mass flow of liquid introduced into the pipe is dragged by the gas, there will be a relationship between the liquid superficial velocity and the liquid film superficial velocity

$$J_{lf} = (1 - E)J_l \quad (17)$$

where  $E$  is the entrained fraction, which is defined as the mass flow of liquid dragged by the gas divided by the total mass flow of liquid. Consequently

$$Re_l = \frac{\rho_l J_l D}{\mu_l} = \frac{\rho_l J_{lf} D}{\mu_l (1 - E)} = \frac{Re_{lf}}{1 - E} \quad (18)$$

and the gas Reynolds number is almost equal in both cases, at the inlet of the pipe and in the region of the developed flow (in both cases almost all the pipe diameter is occupied by the gas), then the only definition of the gas Reynolds number is

$$Re_g = \frac{\rho_g J_g D}{\mu_g} \quad (19)$$

Fukano's experimental conditions were as follows: vertical upward annular flow, inner pipe diameter 26 mm, tube length 4.5 m, superficial gas velocity 10–50 m/s, superficial liquid velocity 0.04–0.3 m/s, system pressure 0.103–0.117 MPa, air and liquid temperature 27–29 °C.

An expression proposed by Hori et al., which also appears in Fukano's work, is

$$\frac{\delta}{D} = 0.905 Re_g^{-1.45} Re_l^{0.90} Fr_g^{0.93} Fr_l^{-0.68} \left( \frac{\mu_l}{\mu_{l,ref}} \right)^{1.06} \quad (20)$$

where  $Re_l$ ,  $Re_g$ ,  $Fr_l$ ,  $Fr_g$  are the Reynolds and Froude numbers of liquid and gas phases, respectively, which are defined from the superficial velocities of gas and liquid phases;  $\mu_l$  and  $\mu_{l,ref}$  are the liquid viscosity of the used liquid at the experimental conditions and a liquid dynamic viscosity reference value of water at a temperature of 20 °C, respectively.  $Re_l$ ,  $Re_g$  and  $Fr_g$  have been defined in Eq. (14), Eq. (15) and Eq. (19), respectively, and  $Fr_l$  is defined, in the same way as in the previous case, as follows

$$Fr_l = \frac{J_l}{\sqrt{gD}} \quad (21)$$

**2.2.1.3. Henstock's and Tatterson's correlations** (Henstock and Hanratty, 1976; Tatterson et al., 1977). Other researchers correlated data against additional terms to include effects other than film Reynolds number. Henstock and Hanratty (1976) correlated the film thickness against a limited set of horizontal and vertical air–water data. They found that the vertical data ( $Re_{lf} \sim 10$ –10,000) were best fitted using

$$\frac{\delta}{D} = \frac{6.59F}{(1 + 1400F)^{0.5}} \quad (22)$$

while their horizontal data ( $Re_{lf} \sim 1000$ –10,000) were best fitted using

$$\frac{\delta}{D} = \frac{6.59F}{(1 + 850F)^{0.5}} \quad (23)$$

the parameter  $F$  can be defined in two ways, one proposed by the own Henstock and a subsequent amendment from Tatterson. These are expressed, respectively, by

$$F = \frac{1}{\sqrt{2}Re_g^{0.4}} \frac{Re_l^{0.5}}{Re_g^{0.9}} \frac{\mu_l}{\mu_g} \frac{\rho_g^{0.5}}{\rho_l^{0.5}} ; \quad F = \frac{\gamma(Re_{lf})}{Re_g^{0.9}} \frac{\mu_l}{\mu_g} \frac{\rho_g^{0.5}}{\rho_l^{0.5}} \quad (24)$$

where

$$\gamma(Re_{lf}) = \left[ \left( 0.707 Re_{lf}^{0.5} \right)^{2.5} + \left( 0.0379 Re_{lf}^{0.9} \right)^{2.5} \right]^{0.4} \quad (25)$$

being  $Re_{lf}$  the Reynolds number of the liquid film flowing in the wall layer, defined as in Eq. (3).

**2.2.1.4. Roberts' correlation** (Roberts et al., 1997). Next expression is a correlation proposed by Spurrett to calculate the film thickness at the bottom of a horizontal pipe. This expression correlates the data of Sekoguchi taken in pipes of diameter 0.026 m

$$\delta = 846 \frac{Re_{lf}^{0.44}}{Re_g^{0.59}} \quad (26)$$

where  $Re_{lf}$  and  $Re_g$  are the Reynolds numbers based on the film velocity, determined using the entrained fraction correlation of Asali (Azzopardi, 1997), and the superficial gas velocity, respectively.

Then Roberts, following Jepson's reasoning (Roberts et al., 1997), assumed that the value of  $\delta/D$  is the same for all the pipes with the same superficial velocities, which allows the calculation of the film thickness at the bottom of a pipe of diameter  $D$ , in meters, given by the expression

$$\delta = 846 \frac{D}{D_{ref}} \frac{Re_{lf}^{0.44}}{Re_g^{0.59}} \quad (27)$$

where  $D_{ref}$  is a reference diameter equal to 0.026 m.

**2.2.1.5. Okawa's correlation** (Okawa et al., 2002). The authors propose to estimate the liquid film thickness from a balance between the interfacial shear force and the wall friction force acting on the liquid film

$$\delta = \frac{1}{4} \sqrt{\frac{f_w \rho_l}{f_{gi} \rho_g}} \frac{J_{lf}}{J_g} D \quad (28)$$

being  $f_w$  the wall friction factor, evaluated with max. (16/ $Re_{lf}$ , 0.005);  $f_{gi}$  is the interfacial friction factor, and the authors recommended to calculate it by using Wallis correlation, Eqs. (7) and (8);  $J_{lf}$  and  $J_g$  are the liquid film and gas superficial velocities.

**2.2.1.6. Ishii and Grolmes' correlation** (Ishii and Grolmes, 1975). The authors propose to estimate the liquid film thickness by the following correlation

$$\delta = 0.347 Re_{lf}^{2/3} \sqrt{\frac{\rho_l}{\tau_i}} \frac{\mu_l}{\rho_l} \quad (29)$$

being  $Re_{lf}$  the Reynolds number of the liquid flowing in the wall layer, defined as in Eq. (3).

They derived this criterion for the roll-wave mechanism by considering a force balance between the drag force,  $F_D$ , from the gas acting on a wave crest on the film, and the retaining force of the surface tension,  $F_\sigma$ .

## 2.2.2. Base liquid film thickness

Observations made by several researchers indicate that liquid film can be divided into two layers (Levy, 1999), a continuous layer and a disturbed wavy layer. Base film thickness is the liquid layer from wall to wave trough, see base film,  $\delta_b$ , in Fig. 3. A correlation

proposed by Dobran (Levy, 1999; Mantilla, 2008) and tested for upward and downward vertical flows is

$$\delta_b = D \left( 140 G_r^{-0.2165} Re_\alpha^{-1.35} \right) \quad (30)$$

where  $G_r$  is a two-phase Grashoff number and  $Re_\alpha$  is the gas core Reynolds number, defined as

$$G_r = \frac{g D^3 \rho_l (\rho_l - \rho_\alpha)}{\mu_l^2} \quad (31)$$

and

$$Re_\alpha = \frac{J_g \rho_\alpha D}{\mu_g} \quad (32)$$

being  $J_g$  the superficial gas velocity and  $\rho_\alpha$  the core density, given by

$$\rho_\alpha = \alpha \rho_g + (1 - \alpha) \rho_l \quad (33)$$

$\alpha$  being the void fraction. The Dobran's expression has been obtained from correlating data of vertical upward and downward flows, and for different tube diameters.

From Eq. (30) it can be observed that all parameters are almost constant when carrying out an experiment under certain conditions. Then, the major source of variation in the above expression is the gas velocity, being the thickness of the base liquid layer an inverse function of this variable. As it is confirmed from several experimental works, it can be said that the wave base height decreases with the gas mass flux. For instance, Han et al. (2006) show that, when the gas mass flux is doubled, the wave base height decreases about 18%.

A first approximation to the base liquid film thickness correlation is presented in the PhD work of Schubring (2008). The correlation is shown below

$$\delta_b = 4.8 D Re_g^{-0.6} \quad (34)$$

### 2.2.3. Wave amplitude

The wave roughness height or wave amplitude can be defined as the distance between the wave base height or base film thickness and the wave peak height. In order to estimate the wave amplitude, the Kelvin-Helmholtz instability has been taken into account. Under this kind of instability, the wave is caused by the relative motion of two continuous phases (Chandrasekhar, 1981). For that instability, the most unstable wave amplitude is (for gas as a continuous phase)

$$\Delta h_{w,K-H} = 3\pi \frac{\left(1 + \frac{\rho_g}{\rho_d}\right) \sigma_l}{\rho_g (u_g - u_l)^2} \quad (35)$$

Holowach et al. (2002) proposes an expression for the wave amplitude that is dependent on fluid properties and interfacial shear. This methodology comes from Ishii and Grolmes (1975), which assumes that the motion of the wave crest with respect to the liquid film can be expressed by a shear flow model. The model is an approximation for the case of wave formation in vertical annular flow, given that gravitational forces are neglected since this analysis calculates the wave height in the radial direction. Then, the proposed expression is

$$\Delta h_w = \frac{\sqrt{2} C_W \mu_l}{(\rho_l \tau_i f_{li})^{1/2}} \quad (36)$$

being  $\tau_i$  the interfacial shear stress, whose expression is presented later on;  $C_W$  is a factor that accounts for the effect of the surface

tension on the circulation/dissipation flow in the wave, and it was defined by Ishii and Grolmes (1975) as follows

$$\begin{aligned} C_W &= 0.028 N_\mu^{-4/5} && \text{for } N_\mu \leq 1/15 \\ C_W &= 0.25 && \text{for } N_\mu > 1/15 \end{aligned} \quad (37)$$

where  $N_\mu$  (originally used by Hinze, 1955) is the viscosity number, which compares the viscous force induced by an internal flow to the surface tension force, defined as

$$N_\mu = \frac{\mu_l}{\left( \rho_l \sigma \sqrt{\frac{\sigma}{g \Delta \rho}} \right)^{1/2}} \quad (38)$$

The interfacial liquid friction factor,  $f_{li}$ , is calculated using the correlation developed by Hughmark (1973). Thus

$$\sqrt{f_{li}} = K Re_{lf}^m \quad (39)$$

where  $K$  and  $m$  are given by

$$\begin{aligned} K &= 3.73, m = -0.47 && \text{for } 2 < Re_{lf} < 100 \\ K &= 1.962, m = -1/3 && \text{for } 100 < Re_{lf} < 1000 \\ K &= 0.735, m = -0.19 && \text{for } 1000 < Re_{lf} \end{aligned}$$

For the wave amplitude calculation the author proposes the liquid interfacial friction factor presented above for  $Re_{lf} > 1000$ , and for the interfacial shear stress, an expression defined by the gas core mixture properties

$$\tau_i = \frac{f_{gi} \rho_\alpha J_\alpha^2}{2} \quad (40)$$

where all magnitudes are based on the superficial gas core mixture properties, and their expression is

$$J_\alpha = \frac{G_g}{\rho_g} + \frac{G_e}{\rho_l} \quad (41)$$

being  $G_g$  and  $G_e$  the gas and entrained mass fluxes, respectively. On the other hand, the interfacial gas friction factor is defined as

$$f_{gi} = 0.079 Re_\alpha^{-1/4} \left[ 1 + 24 \left( \frac{\rho_l}{\rho_g} \right)^{1/3} \frac{\delta}{D} \right] \quad (42)$$

In this case  $Re_\alpha$  is the gas core Reynolds number, defined as

$$Re_\alpha = \frac{(G_g + G_e) D}{\mu_g} \quad (43)$$

Han et al. (2006) performed an experimental work in a vertical pipe of 9.525 mm, in which liquid mass fluxes were ranging from 126 to 198 kg/m<sup>2</sup>s and gas mass fluxes were ranging from 18 to 47 kg/m<sup>2</sup>s. The correlation proposed by the authors can be approximated as follows

$$\Delta h_w = 4000 D Re_g^{-1.12} \quad (44)$$

Han's experimental measurements confirm that the peak height (sum of the base liquid film thickness and the wave amplitude) decreases when the gas mass flux increases, but to a greater extent than in the previous case of the base thickness. In fact, he shows that when the gas mass flux is doubled, the wave peak height decreases by about 43%.

### 2.2.4. Wave celerity

The next parameter that will be presented is the wave celerity. Several expressions are presented, such as the ones proposed by Kumar, Pearce, Swanson and Marmottant.

Kumar ([Mantilla, 2008](#)) proposed a model where the wave velocity or celerity is obtained by calculating the interfacial friction factors based on the gas velocity and liquid velocity. Equating the two interfacial friction factors, the interfacial velocity (wave celerity) is determined as follows

$$c = \frac{\psi \cdot J_g + J_l}{1 + \psi} \quad (45)$$

where  $\psi$  is obtained from the next expression

$$\psi = \sqrt{\frac{\rho_g f_{gi}}{\rho_l f_{li}}} \quad (46)$$

being  $f_{li}$  and  $f_{gi}$  the liquid and gas interfacial friction factors. However, they proposed the following empirical correlation to estimate this parameter

$$\psi = 5.5 \sqrt{\frac{\rho_g}{\rho_l}} \left( \frac{Re_l}{Re_g} \right)^{0.25} \quad (47)$$

Pearce's correlation is given by the following expression ([Alamu, 2010](#))

$$c = \frac{KV_l + J_g \sqrt{\frac{\rho_g}{\rho_l}}}{K + \sqrt{\frac{\rho_g}{\rho_l}}} \quad (48)$$

being

$$V_l = \frac{DG_l(1 - E)}{4\rho_l \delta} \quad (49)$$

$G_l$  is the total liquid mass flux,  $E$  is the entrained fraction and  $\delta$  is the liquid film thickness. The Pearce coefficient,  $K$ , is function of pipe diameter and inlet conditions. The value used by Alamu for the  $K$  factor varies between 0.3 and 0.65, depending on the correlated data.

Omebere-Iyari and Azzopardi ([Omebere-Iyari and Azzopardi, 2007; Sawant et al., 2008b](#)) correlated, using the Pearce's correlation, a database of disturbance wave velocity, and they also evaluated the diameter dependence of Pearce coefficient. The authors found that  $K$  increases from 0.51 to 0.9 when the pipe diameter increases from 0.5 to 2.5 cm. Between 2.5 and 4.2 cm, the value of  $K$  remains constant in 0.9.

Swanson ([Schubring and Shedd, 2008](#)) found that the gas friction velocity was equal to the wave celerity for his databank. The gas friction velocity is defined as follows

$$u_g^* = \sqrt{\frac{\tau_w}{\rho_g}} \quad (50)$$

being  $\tau_w$  the wall shear stress.

Marmottant and Villermaux ([Belt et al., 2010](#)) performed a theoretical study on co-axial jets, whose configuration was in fact very similar to that of annular flow. They showed that a shear instability governs the large waves on the jet. The linear shear instability analysis provides an equation for the wave velocity

$$c = \frac{\sqrt{\rho_g} J_g + \sqrt{\rho_l} J_l}{\sqrt{\rho_g} + \sqrt{\rho_l}} \quad (51)$$

This equation is obtained with the assumption  $J_g \gg J_l$ .

[Schubring and Shedd \(2009\)](#) propose a correlation to determine the wave velocity in horizontal annular flow

$$c = 0.41 \frac{J_g}{\sqrt{x}} Re_g^{-0.25} \quad (52)$$

being  $x$  the gas dynamic quality, quotient between gas mass flow rate and the total mass flow rate, given by

$$x = \frac{\dot{m}_g}{\dot{m}_g + \dot{m}_l} \quad (53)$$

The author says that the performance of this correlation is good enough for all diameters studied. Even though, he says that the effect of gas flow is not entirely grasped, as the measured wave velocities vary over a somewhat narrower range than the correlated values do.

[Al-Sarkhi et al. \(2012\)](#) explains that wave celerity is a strong function of the superficial liquid and gas velocities, being also dependent on the inclination angle. They propose three different correlations for the horizontal: the inclination angles from 10° to 20°, the inclination angles of 45° and up to 90° cases. These expressions are, respectively

$$\frac{c}{J_l} = 2.379 \cdot X^{-0.9} \quad (54)$$

$$\frac{c}{J_l} = 2.323 \cdot X^{-0.94} \quad (55)$$

$$\frac{c}{J_l} = 1.942 \cdot X^{-0.91} \quad (56)$$

being  $X$  the Lockhart–Martinelli number, defined as

$$X = \sqrt{\frac{\rho_l J_l^2}{\rho_g J_g^2}} \quad (57)$$

### 2.2.5. Wave Frequency

A wave frequency correlation for disturbance waves has been proposed by Azzopardi ([Azzopardi, 2006; Mantilla, 2008](#)). This expression is a relationship between the Strouhal number (dimensionless wave frequency) and the Lockhart–Martinelli number

$$St_l = 0.25X^{-1.2} \quad (58)$$

where  $St_l$  and  $X$  are the liquid Strouhal number and the Lockhart–Martinelli number, respectively. The Strouhal number is defined as

$$St_l = \frac{vD}{J_l} \quad (59)$$

being  $v$  the wave frequency.

Another empirical correlation for wave frequency in terms of Strouhal number has been obtained by [Alamu \(2010\)](#). He used a curve-fitting method based on his own data. This correlation is very similar to the one presented above, and is given by

$$St_l = 0.4292X^{-0.908} \quad (60)$$

Alamu's experimental data have been obtained in a vertical pipe in upward flow conditions and with a water–glycerin mixture as working liquid.

Azzopardi (Al-Sarkhi et al., 2012) proposes a quite similar expression for the wave frequency

$$St_l = 1.1X^{-0.93} \quad (61)$$

Hazuku et al. (Sawant et al., 2008b) measured the frequency of disturbance waves in vertical annular flow experiments performed at atmospheric pressure condition in 1.1 cm diameter pipe and using as working fluids water and air. They were able to correlate their disturbance wave frequency data with Sekoguchi's expression, and the values were within  $\pm 25\%$  of deviation. The Sekoguchi's correlation is as follows

$$St_g = \frac{vD}{f_g} = f_1(Eo)f_2(Re_l, Fr_g) \quad (62)$$

where  $Eo$  and  $Fr_g$  are the Eötvös and the Froude numbers, respectively, which are defined as

$$Eo = \frac{gD^2(\rho_l - \rho_g)}{\sigma} \quad (63)$$

and the Froude number which has been defined in Eq. (14). Being  $f_1$  and  $f_2$  given by

$$\begin{aligned} f_1(Eo) &= Eo^{-0.5}[0.5Ln(Eo) - 0.47] \\ f_2(Re_l, Fr_g) &= 0.0076Ln\left(\frac{Re_l^{2.5}}{Fr_g}\right) - 0.051 \end{aligned} \quad (64)$$

Although, as it has been said by Sawant, the presented correlation successfully predicts the low-pressure data, it failed to predict the high-pressure data. Therefore, the following new correlation was proposed

$$St_g = 0.086Re_l^{0.27}\left(\frac{\rho_l}{\rho_g}\right)^{-0.64} \quad (65)$$

where the adjustment constants are obtained based on the Sawant's experimental data, using regression analysis. This correlation predicts their experimental data for all pressure conditions within  $\pm 25\%$  deviation. They also correlated Schadel's (carried out with air–water) and Willetts's (carried out with air–water and helium–water at 1.5 bar) experimental data and they were predicted satisfactorily.

In Alamu's PhD thesis (Alamu, 2010) an expression quite similar to Sawant's correlation is also presented

$$St_g = 0.009f_g\left(\frac{\rho_l}{\rho_g}\right)^{0.5} \quad (66)$$

This expression has been obtained by fitting his experimental data points.

### 3. The onset of entrainment process

For low relative velocities between liquid and gas phases, there is a smooth interface. As this difference in velocity increases, the interface covers with waves and, from a certain point, part of the liquid is dragged by the gas phase, this is called the "onset of entrainment". The processes that take place on the gas–liquid interface are at dynamic equilibrium with continuous exchange of mass, momentum and energy between the liquid film and the gas

stream. The liquid in the film continuously enters the gas core in the form of droplets, in a process called liquid entrainment, and the droplets in the gas core continuously deposit on the film, in a process called droplet deposition. When the mass flow rate of entrained and deposited droplets equals, that is to say the mass of liquid droplets remains constant in the gas core, the fully developed annular flow is achieved. The ratio of the mass flow rate of the liquid phase, in the form of droplets in the gas core, to the total mass flow rate of the liquid phase is defined as the liquid entrainment fraction.

The deformation mechanisms in the gas–liquid interface are caused by a force balance. The hydrodynamic and the surface tension forces govern the motion and deformation of the disturbance waves. Under certain conditions, this force balance leads to an extreme deformation of the interface, which results in breakup of a portion of a wave into several liquid droplets; this point is the onset of entrainment. These droplets can be entrained into the gas core in several different ways. There are five basic types of entrainment mechanisms (Ishii and Grolmes, 1975) and all of them can occur in concurrent flow except the last one. These mechanisms are: roll wave, wave undercut, bubble bursting, liquid impingement and liquid bulge disintegration; all of them are shown in Fig. 4.

It is important to remark that for low viscous fluids, as water, the dominant mechanism of liquid entrainment into the gas core flow is the roll wave, but wave undercut mechanism is also possible for low liquid Reynolds numbers. This statement is supported by the findings of Van Rossum (1959), Hall-Taylor et al. (1963), Woodmansee and Hanratty (1969) and Schadel (1988); consequently only the roll wave mechanism is analyzed in the present article. In this mechanism, the drag force acting on the wave tops deforms the gas–liquid interface, shearing off the tops of large amplitude roll waves by the turbulent gas flow. The relation between the disturbance waves and droplet entrainment processes has been established since the 60s by several methods and authors (Cooper et al., 1964; Jacowitz and Brodkey, 1964; Arnold and Hewitt, 1967; Woodmansee and Hanratty, 1969). However, the exact mechanism for how the liquid droplets are generated out of a disturbance wave is still controversial.

In the entrainment mechanisms, when a gas phase is flowing over a liquid film, the gas–liquid interface may become unstable depending on the magnitude of the gas and liquid velocities. For a

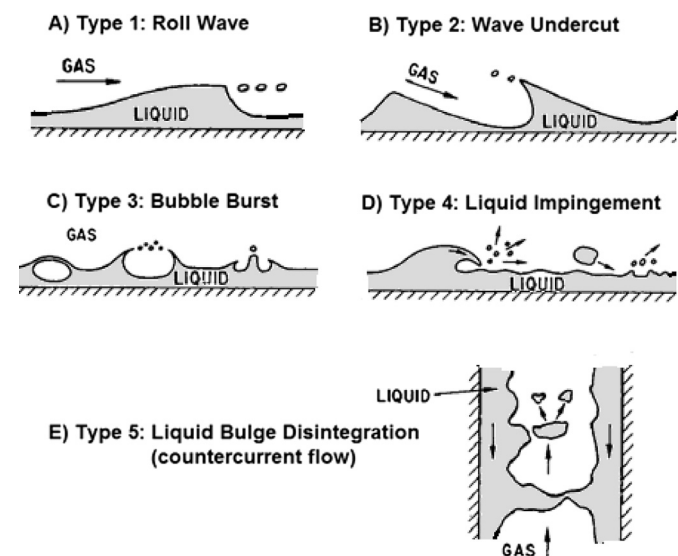


Fig. 4. Entrainment mechanisms in concurrent two-phase flow.

very small gas velocity, the interface is relatively stable. However, as the gas velocity increases, the interfacial wave appears as result of the Kelvin–Helmholtz instability. The amplitude and irregularity of the waves become more and more pronounced as the gas velocity is further increased. At a sufficiently high gas flow, the interfacial waves transform into large amplitude roll waves. Beyond this point, the interfacial shear forces become greater than the surface tension forces and the onset of entrainment occurs. The critical condition for entrainment to take place depends on the liquid film Reynolds number and on the gas stream velocity, see Fig. 5.

In the 50s and 60s, considerable theoretical and experimental works were carried out on the study of the onset of entrainment (OE) and on the onset of disturbance waves (ODW) (Hanratty and Engen, 1957; Van Rossum, 1959; Hanratty and Hershman, 1961; Zhivaikin, 1962; Cousins et al., 1965), and all of them point out that the large amplitude DW disappear at the OE. The conclusion made by these researchers is that the OE and ODW conditions are always similar. This assumption has been confirmed subsequently by other researchers, for instance Ishii and Grolmes (1975), Azzopardi (1997) and Hills (1997).

The value of the liquid film Reynolds number corresponding to that DW transition, the onset of entrainment Reynolds number,  $Re_{OE}$ , is not firmly established. However, the results of the various investigations for low viscous liquids suggest that the onset of entrainment Reynolds number is in the range of 2 for vertical downward flows. For horizontal and vertical upward flows, which are the most widely studied due to its industrial importance, the onset of entrainment Reynolds number is between 100 and 400 approximately, depending on the author. For instance, Ishii and Grolmes (1975) suggest a value of 160; Abolfadl (Azzopardi, 1997) linked the start of entrainment with the onset of turbulence in the film, then he specified a value to the onset of entrainment Reynolds number of 268 based on its available experimental data; Okawa et al. (2003) takes a critical value of 320 from experimental data. Lower values are proposed by other authors, for instance, Nigmatulin (Alipchenkov et al., 2004) proposes a value for the onset of entrainment Reynolds number of 180, Andreussi et al. (1985) suggest a value of 94 approximately, Azzopardi (Azzopardi, 1983; Lopez de Bertodano et al., 1998) gave a value of 80 based on wave inception results for both Freon and water.

The transition also depends on the gas flow. Under high gas velocity condition, the ODW correspond to the values at which OE is produced, that condition corresponds to a limiting value of the liquid Reynolds number, the so called onset of entrainment

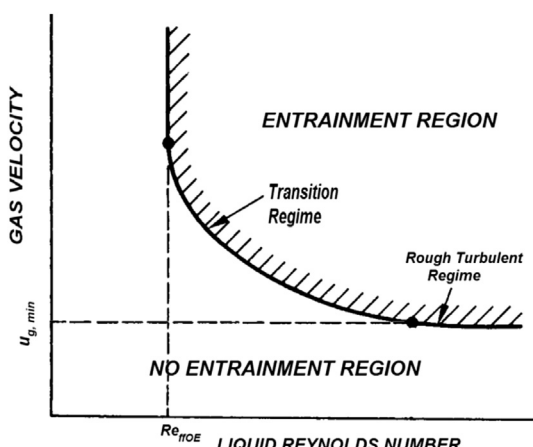


Fig. 5. Schematic entrainment inception velocity boundary for each particular combination of liquid and gas conditions.

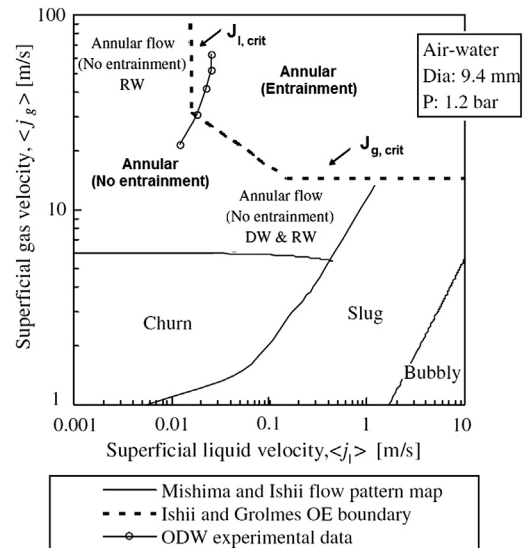


Fig. 6. Vertical upward annular two-phase flow pattern map (Sawant et al., 2009).

Reynolds number. As it has been explained previously, for low viscous fluids, this transition occurs at approximately Reynolds numbers of 160 (Ishii and Grolmes, 1975); but it has been also proposed that, for  $Re_{OE} < 160$ , suppression of entrainment takes place due to the suppression of DW (Azzopardi, 1983; Alipchenkov et al., 2004; Andreussi et al., 1985). Although the works of other researchers suggest higher values for this  $Re_{OE}$  (Owen and Hewitt, 1987; Azzopardi, 1997; Pan and Hanratty, 2002b; Sawant et al., 2009), they explain that the asymptotic liquid velocity or the critical liquid velocity at ODW is higher than the prediction of Ishii and Grolmes criterion. Otherwise, a careful examination of the limited experimental data on the inception of entrainment indicates that there exists a deviation from the criterion based on the DW mechanism when the gas velocity is not high enough, see Fig. 6. So, at lower gas velocity, the trends presented by ODW and OE conditions are opposite. The ODW boundary shows that the liquid velocity at ODW decreases with the decreasing gas velocity and the OE boundary shows the liquid velocity at the OE increases with the decreasing gas velocity. Thus, it appears that, only under high gas velocity, the conditions for OE and ODW are similar, and only under these conditions the  $Re_{OE}$  can be employed.

As it has been presented in the previous paragraph, the  $Re_{OE}$  corresponds to the critical liquid film flow rate at which OE takes place under high gas velocity condition. For horizontal and vertical upward annular flows, a value of 160 for the  $Re_{OE}$  can be chosen as a first approximation for this transition, even though several expressions to obtain this value are presented in the next paragraphs.

Pan and Hanratty (2002a,b) developed an entrainment correlation for liquids with viscosities close to that of water, based on a balance between the rates of atomization and deposition. Both the gravity and droplet size effects are considered in the correlation. This correlation for horizontal flow, as well as the one for vertical flows, is the only correlation that considers explicitly the concept of critical liquid film rate. This liquid critical flow is the liquid flow above which the initiation of atomization occurs, that is, when disturbance waves appear on the liquid layer, the so called onset of entrainment condition. Measurements of Andreussi et al. (1985) of the liquid flow needed to initiate disturbance waves in vertical flows can be used to calculate the critical flow per unit length,  $\Gamma_{lfc} = W_{lfc}/\pi D$ , where  $W_{lfc}$  is the critical film flow rate below which atomization does not occur. The calculation of that critical flow rate

employs the onset of entrainment Reynolds number. These two magnitudes are represented by the following equations

$$Re_{ffOE} = 7.3(\log_{10}\omega)^3 + 44.2(\log_{10}\omega)^2 - 263(\log_{10}\omega) + 439 \quad (67)$$

where the onset of entrainment Reynolds number can be written as

$$Re_{ffOE} = \frac{4\Gamma_{lfc}}{\mu_l} \quad (68)$$

and

$$\omega = \frac{\mu_L}{\mu_g} \sqrt{\frac{\rho_g}{\rho_l}} \quad (69)$$

For air and water at standard conditions,  $\omega = 1.861$  and  $Re_{ffOE} = 370$ . Measurements in horizontal flows, by Dallman (1978) and by Laurinat (1982), suggest larger values of  $\Gamma_{lfc}$  by a factor of about 1.3, probably because of the asymmetry of the liquid layer. Eq. (67) was derived from measurements for  $\omega = 1.8$  to 28, and it should not be used outside this range.

Another expression to calculate the critical Reynolds number,  $Re_{ffOE}$ , is the one proposed by Owen (Owen and Hewitt, 1987; Jiao et al., 2009). In that equation, the Reynolds number above which entrainment happens is obtained as follows

$$Re_{ffOE} = \exp \left( 5.8405 + 0.4249 \frac{\mu_g}{\mu_l} \left( \frac{\rho_l}{\rho_g} \right)^{0.5} \right) \quad (70)$$

Azzopardi (1997) presented a review of experimental data on measurement of ODW and OE conditions, and correlations available for the prediction of these conditions (Table 1). In the existing experimental data there is a reasonable range of liquid viscosity, surface tension and pipe diameter covered, but all the experiments were carried out at or near atmospheric pressure. The database covered a range of pipe diameter from  $16 \times 10^{-3}$  to 0.125 m and a range of viscosity from 1.0 to  $24.4 \times 10^{-3}$  Pa s. He found that the existing correlations for ODW failed to predict the diameter and viscosity effects.

Later on, experiments of Sawant et al. (2008a, 2009) covered higher pressure conditions, 1.2, 4.0 and 6.0 bar, a range of diameters from 0.94 to 12.5 cm, and a range of liquid viscosities from 1 to  $24 \times 10^{-3}$  Pa s. They concluded that previous non-dimensional numbers failed to predict the pressure effects or density ratio changes observed in their data. Using the viscosity number ( $N_\mu$ , originally used by Hinze, 1955, defined in Eq. (38), which compares the viscous force induced by an internal flow to the surface tension force), they were able to collapse their data and a database of experimental measurements, all of them with  $D \leq 3.2$  cm. And under high gas velocity conditions, the non-dimensional group  $Re_{lf}N_\mu^{0.5}$  asymptotically approaches a value of 13. Since the conditions of OE or ODW under high gas velocity are similar, a new correlation for  $Re_{ffOE}$  can be given as follows

$$Re_{ffOE} = 13N_\mu^{-0.5} \quad (71)$$

Observations of Andreussi et al. (1985) of the conditions for the initiation of roll waves are shown in Fig. 7. These results also clearly show that, at large gas velocities, the transition is approximately independent of gas flow. As can be observed from the figure, the results for the critical condition at large gas velocities are given by  $Re_{ffOE} \approx 95$ , instead of the previously higher values presented above. However, he also explains that good agreement between this calculation and experiment is obtained at high liquid Reynolds

**Table 1**

Critical Liquid Reynolds numbers for wave inception at high gas velocity conditions (Azzopardi, 1997).

Author	Experimental	Asali	Owen and Hewitt	Ishii and Gromes
Azzopardi et al. (1983)	211	290	429	58
Martin (1983)	245	272	412	43
Whalley et al. (1977)	330/360	272/284	412/423	43/53
Azzopardi, 1997	255	284	423	53
Shearer (1964)	282/300	231/272	383/411	22/46
Asali (1984)	205–240	225	261/345	7/40
Hall-Taylor and Nedderman (1968)	105/298	225/284	351/423	1.8/53

numbers, but the film is more stable than the calculated for low liquid Reynolds numbers.

The entrainment process occurs, under high gas velocity condition, when the liquid film Reynolds number, defined by Eq. (18), is bigger than the onset of entrainment Reynolds number

$$Re_l > Re_{ffOE} \quad (72)$$

Then, finally, the critical liquid film velocity above which entrainment occurs can be expressed as

$$J_l = Re_{ffOE} \frac{\mu_l}{\rho_l D} ; u_l = Re_{ffOE} \frac{\mu_l}{\rho_l 4\delta} \quad (73)$$

being  $u_l$  and  $J_l$  the liquid film and superficial liquid film velocities, respectively.

#### 4. The entrainment inception velocity

The onset of entrainment Reynolds number, presented in the previous section, only shows the limiting value of the liquid film velocity under which no entrainment is possible. This value is regardless of the gas flow conditions, but does not indicate the critical gas velocity above which entrainment takes place when liquid film number is above its critical value. This critical gas velocity is the entrainment inception velocity.

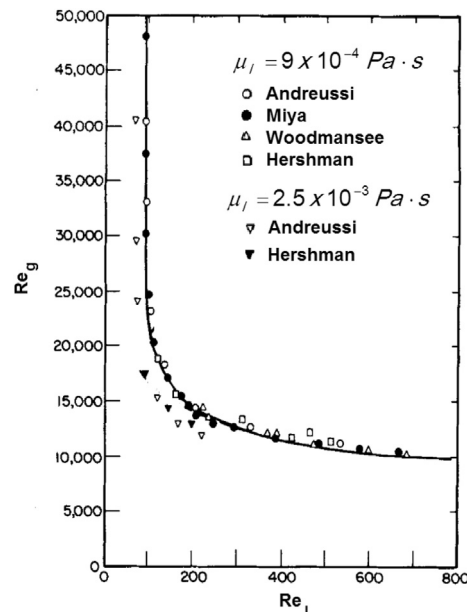


Fig. 7. Effect of gas and liquid Reynolds numbers on roll wave transition (Andreussi et al., 1985).

The entrainment inception velocity is the gas critical velocity above which the entrainment process can take place. Different models have been developed in the course of time, the most widely used are the Kutateladze criterion and the Ishii and Grolmes model, but many others are available in the literature. Next sections are devoted to the description of many of these entrainment inception expressions.

#### 4.1. Kutateladze number criterion

Abundant work on the inception velocity can be found in the two-phase flow domain. However, in most cases, evaluation sustained by theoretical considerations is provided for a gas flowing over a pool or a liquid film. In the Epstein paper (Epstein, 1990), it is obtained from the Kutateladze number criterion ( $Ku > 3.1$ ). This model gives as a result a constant velocity value above which entrainment takes place

$$Ku^2 = \frac{\rho_g u_g^2}{\sqrt{\sigma g \rho_l}} \geq 9.61 \quad (74)$$

Then, working out the values of the velocity, the limiting gas velocity is given by

$$u_g \geq \sqrt{\frac{9.61 \sqrt{\sigma g \rho_l}}{\rho_g}} \quad (75)$$

Note that the Kutateladze number may be written as a Weber number

$$Ku^2 = \frac{\rho_g u_g^2}{\sigma} \sqrt{\frac{\sigma}{g \rho_l}} = \frac{\rho_g u_g^2}{\sigma} l_{\text{interf}} = We_{\text{interf}} \quad (76)$$

where  $l_{\text{interf}} = \sqrt{\sigma/g \rho_l}$  is a characteristic length in the interface stability theory. In this approach, only the interfacial tension and gravity acceleration are considered, and not the liquid viscosity.

The above criterion gives a constant entrainment inception velocity value depending only on gas and liquid properties. An improvement of the previous model is the one proposed by Crowe (2006). In that model, three regions are considered.

1. No entrainment zone. Reynolds numbers under  $Re_{\text{ffOE}}$ , where entrainment is not possible
2. Rough turbulent zone. Liquid film Reynolds number exceeds a value of about 1500–1750, the liquid film flow becomes completely rough-turbulent and the entrainment inception velocity has a constant value.
3. Transition zone. Reynolds number between these two values, the entrainment inception velocity has not a constant value

First region, below the  $Re_{\text{ffOE}}$ , see Section 3, where different values of this parameter have been presented. In that region, the critical Kutateladze number has a high value and liquid entrainment is difficult or impossible to achieve.

Second region is the rough turbulent regime (the typical critical value proposed for this region is  $Re_{\text{lf}} = 1635$ ); according with Crowe's suggestions, liquid entrainment is expected to exist in this region for Kutateladze numbers bigger than 3.2 (slightly different Ku number that the one proposed by Epstein)

$$Ku^2 = \frac{\rho_g u_g^2}{\sqrt{\sigma g \rho_l}} \geq 10.24 \quad (77)$$

Then, using the same procedure of the Epstein model, gives as a result the following limiting gas velocity expression

$$u_g \geq \sqrt{\frac{10.24 \sqrt{\sigma g \rho_l}}{\rho_g}} \quad (78)$$

Third region is the transition regime, where the critical Kutateladze number increases with decreasing Reynolds number. Using as a first approximation the value of 160 for the onset of entrainment Reynolds number, and the value of 1635 for the beginning of the rough turbulent region; then the transition regime covers the liquid film Reynolds numbers  $160 < Re_{\text{lf}} < 1635$ . At the lower Reynolds side of the regime, the critical Kutateladze number is  $Ku \approx 7.5$ . So, considering as linear the variation in that transition region

$$Ku^2 = \frac{\rho_g u_g^2}{\sqrt{\sigma g \rho_l}} \geq 61.241 - 0.0312 Re_{\text{lf}} \quad (79)$$

being  $Re_{\text{lf}}$  the liquid film Reynolds number, defined in Eq. (15).

Then, the entrainment inception velocity is

$$u_g \geq \sqrt{\frac{(61.241 - 0.0312 Re_{\text{lf}}) \sqrt{\sigma g \rho_l}}{\rho_g}} \quad (80)$$

#### 4.2. Ishii and Grolmes model

In annular flow, the surface of the liquid film is not smooth but covered with waves, see Ishii and Grolmes (1975). The shape of waves depends on the velocities of liquid and gas phases. The paper of Ishii and Grolmes states that there exists a lower limit of  $Re_{\text{lf}}$ , under which roll-wave entrainment will not take place no matter how high is the gas velocity over the film, the previously presented  $Re_{\text{ffOE}}$ . In the other extreme, at high  $Re_{\text{lf}}$  (rough turbulent regime), the gas velocity necessary for the inception of the entrainment process becomes independent of the liquid film Reynolds number; this regime starts at  $Re_{\text{lf}} \approx 1635$ .

Ishii and Grolmes derived a criterion for the onset of roll-wave entrainment by considering a force balance between the drag force  $F_D$ , from the gas acting on a wave crest on the film, and the retaining force of the surface tension  $F_\sigma$  (Fig. 8). They assumed that roll wave entrainment was possible when the drag forces exceeded the retaining force of the surface tension.

An entrainment inception criterion velocity can be found depending on the viscosity number, Eq. (38), and the liquid film Reynolds number, Eq. (15). For horizontal flow and  $Re_{\text{lf}} > Re_{\text{ffOE}}$  (remember that the authors used for  $Re_{\text{ffOE}}$  a value of 160 for horizontal and vertical upward flow and 2 for vertical downward flow), the inception criterion is

$$\begin{aligned} \frac{\mu J_g}{\sigma} \sqrt{\frac{\rho_g}{\rho_l}} &\geq 11.78 N_\mu^{0.8} Re_{\text{lf}}^{-1/3} && \text{for } N_\mu \leq \frac{1}{15}; Re_{\text{ffOE}} \leq Re_{\text{lf}} \leq 1635 \\ \frac{\mu J_g}{\sigma} \sqrt{\frac{\rho_g}{\rho_l}} &\geq 1.35 Re_{\text{lf}}^{-1/3} && \text{for } N_\mu > \frac{1}{15}; Re_{\text{ffOE}} \leq Re_{\text{lf}} \leq 1635 \end{aligned} \quad (81)$$

where  $J_g$  is the volumetric flux of gas (superficial gas velocity).

For the rough turbulent regime ( $Re_{\text{lf}} > 1635$ ) the inception criterion is

$$\begin{aligned} |J_g| &> \frac{\sigma}{\mu_l} \sqrt{\frac{\rho_l}{\rho_g}} \times N_\mu^{0.8} && \text{for } N_\mu \leq \frac{1}{15}; Re_{\text{lf}} > 1635 \\ |J_g| &> \frac{\sigma}{\mu_l} \sqrt{\frac{\rho_l}{\rho_g}} \times 0.1146 && \text{for } N_\mu > \frac{1}{15}; Re_{\text{lf}} > 1635 \end{aligned} \quad (82)$$

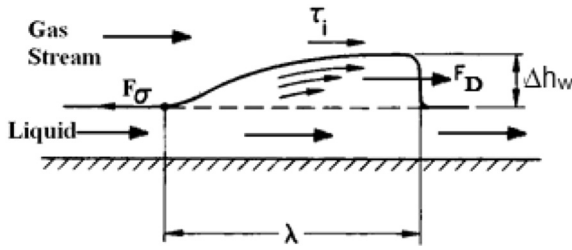


Fig. 8. Side view of entrainment model based on roll-wave breakup.

#### 4.3. Other entrainment inception velocity models

Large discrepancies exist among the different correlations and also between the different experimental data. Hence, the agreement of the simulation results with Ishii and Grolmes correlation is satisfactory. Other correlations are available in the literature, for instance the ones of Kulov, Sawant, etc.

The correlation obtained by Kulov (Yun et al., 2010) is quite simple and it only shows the relation between the gas and liquid velocities. That relation is shown via the gas and fluid Reynolds numbers

$$Re_g = \frac{5.32 \times 10^4}{Re_{lf}^{0.19}} \quad (83)$$

In Fig. 9, the comparison of Yun's numerical simulation versus the Kulov's correlation for the onset of entrainment is shown. The results of the numerical simulation data of Yun et al. (2010) are smaller than the ones of this equation. Most of the data are located between 50 and 100% of the Kulov's correlation values.

In the articles of Sawant et al. (2008a) and Pan and Hanratty (2002a) the following expression to obtain the critical gas velocity at the onset of entrainment is proposed

$$\frac{D^{0.5} J_g (\rho_l \rho_g)^{0.25}}{\sigma^{0.5}} \equiv 40 \quad (84)$$

This correlation is empirical and dimensional, so it is necessary to check its applicability range.

A summary of critical gas velocities obtained by different authors is shown in Table 2 and it summarizes the measurements by Willetts, Wallis, Lopez de Bertodano and Andreussi (Pan and Hanratty, 2002a).

As was explained by Pan, all the studies, with the exception of one, used  $\rho_l = 1000 \text{ kg/m}^3$  and  $\sigma = 0.073 \text{ N/m}$ . His analysis suggest

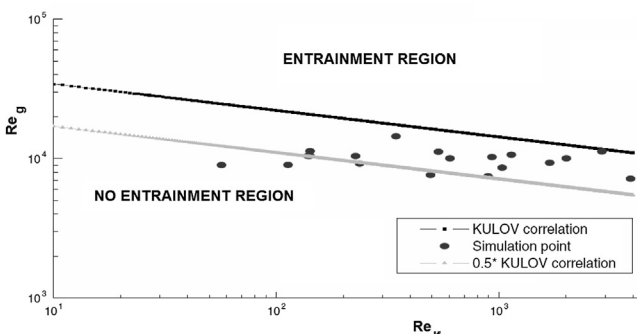


Fig. 9. Comparison of the onset criteria for entrainment based on the Kulov relation and the numerical simulation data of Yun et al. (2010).

that in Eq. (84) should be used  $\rho_g^{0.5}$  rather than  $(\rho_g \rho_l)^{0.25}$ . However, the opposite conclusion would be reached by examining the results of Willetts for air–water and helium–water.

Another expression to obtain the onset of entrainment gas velocity in annular flow has been correlated over a wide database by Hewitt and Hall-Taylor (Flores et al., 1995)

$$u_g = 1.5 \times 10^{-4} \sqrt{\frac{\rho_l}{\rho_g}} \frac{\sigma}{\mu_g} \quad (85)$$

#### 5. Study of experimental data and adjustment correlations

This section is dedicated to present all the studies conducted to determine the most important characteristics of the liquid film layer in annular two-phase flow. In particular, we have concentrated on the determination of the film thickness of this liquid layer, wave celerity and wave frequency. Thus, we have made a division into three subsections. The first one is devoted to the liquid layer thickness, the second to wave velocity (usually called celerity or wave celerity) and the third, and last, to the frequency of these waves. Each subsection is organized as follows: the first part is devoted to present some conclusions drawn directly from the experimental data; the next part presents the empirical correlations found in the literature and the work made to improve them from the available experimental data; and finally, we will present the comparison of all these correlations with the experimental data.

##### 5.1. Thickness of the liquid film layer

A lot experiments have been carried out in the last decades in order to determine the thickness of the liquid film existent in annular flow. In particular, in the present work, we have analyzed the following experimental data series: Tatterson et al. (1977), Cousins and Hewitt (Tatterson et al., 1977), Paras and Karabelas (1991), Schubring (2008) and Alamu (2010); the experimental conditions of each of them will be described below. For Tatterson's data, the measurements were taken with the electrical probe technique in a horizontal channel of 0.305 m high and 0.025 m width. Paras and Karabelas data were obtained in a horizontal pipe

**Table 2**  
Summary of critical gas velocities for different authors (Pan and Hanratty, 2002a).

Author	Fluids	D (cm)	$\rho_g (\text{kg/m}^3)$	$V_g$ (m/s)	$X_E^a$
Willetts (1987)	Air–water	1.026	1.83	22	53
	He–water	1.026	0.27	35	53
	Air–Genklene	1.026	2.41	8	39
Wallis (1968)	Air–water	1.588	1.5	18	53
	(1 atm)		(assumed)		
	Air–water	1.588	3.0	12	42
	(2 atm)		(assumed)		
	Air–water	1.588	4.5	11	41
	(3 atm)		(assumed)		
Lopez de Bertodano and Jan (1998)	Air–water	1.588	6.0	10	41
	(4 atm)		(assumed)		
	Air–water	0.953	1.6	24	54
	(1 atm)		(assumed)		
Lopez de Bertodano et al. (1998) (1997)	Air–water	0.953	2.8	15	40
Andreussi and Zanelli (1976, 1979) (downflow)	Air–water	0.953	4.4	13	39
Andreussi and Zanelli (1976, 1979) (downflow)	Air–water	2.4	1.38	11	39

<sup>a</sup>  $X_E = D^{0.5} J_g (\rho_l \rho_g)^{0.25} / \sigma^{0.5}$ .

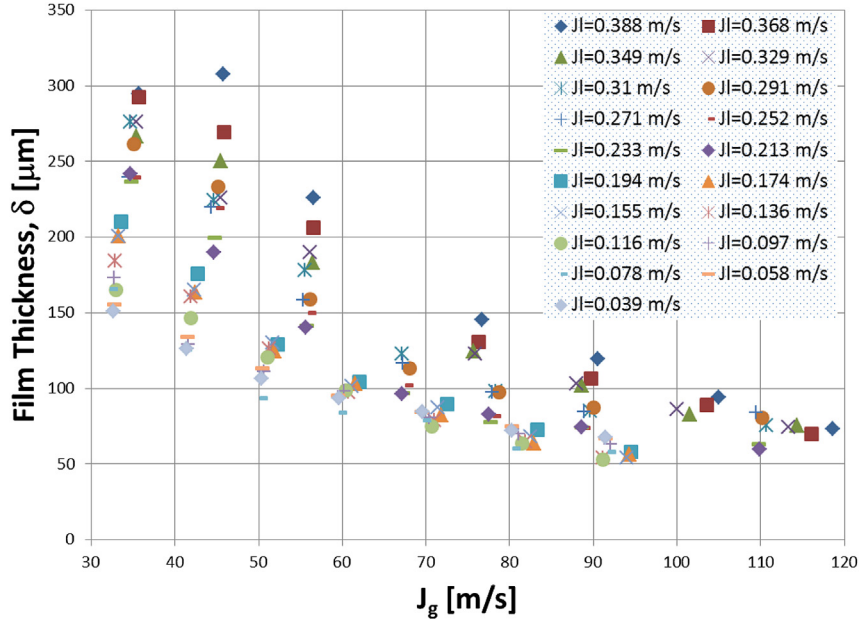


**Fig. 10.** Schubring's experimental liquid film thickness data vs. superficial gas velocity (vertical upward flow,  $D = 0.0234$  m,  $P$  and  $T$  ambient, working fluids: air–water) with constant liquid velocity.

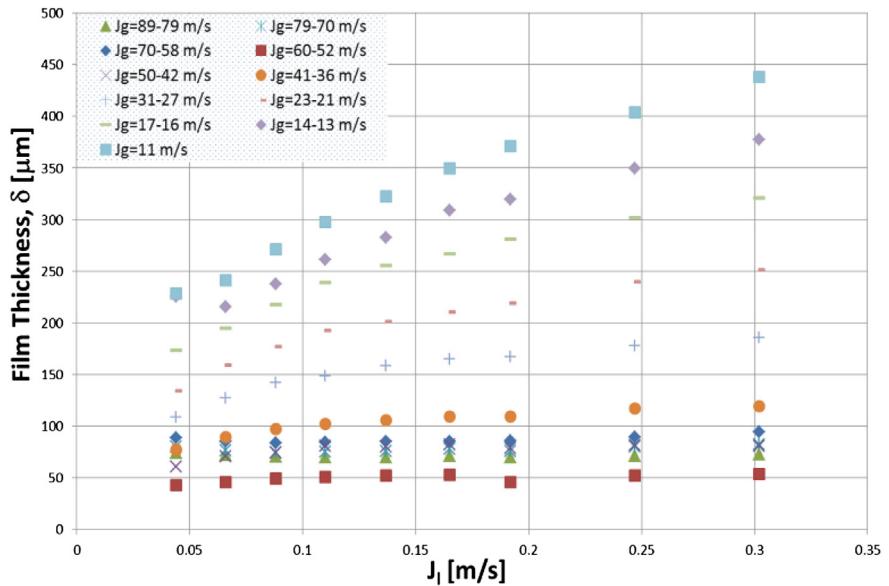


**Fig. 11.** Schubring's experimental liquid film thickness data vs. superficial liquid velocity (horizontal flow,  $D = 0.0088$  m,  $P$  and  $T$  ambient, working fluids: Air–Water) with “constant” gas velocity (actually the gas velocity was somewhat higher for higher liquid mass flows, the range is indicated in the figure legend).

of 5.068 cm of inner diameter; liquid film thickness along the pipe was measured using parallel-wire conductance probes. Schubring's data were taken with an optical technique; this non-intrusive technique uses the pattern of diffuse light reflected from the liquid surface to determine the liquid film thickness; these experimental series covered measurements mainly in horizontal conditions<sup>2</sup> (3 series with inner diameters of 0.88, 1.51 and 2.63 cm,

respectively), but also in vertical upward conditions (pipe of 2.34 cm of inner diameter). Finally, Alamu's data were taken on a vertical pipe with an inner diameter of 1.9 cm, the working fluids were air and a mixture of water and glycerin (dynamic viscosity of 3.6 mPa s and density of 1097 kg), at a pressure of 1.5 bars and ambient temperature.

This section is organized as follows: first, an initial analysis of the available experimental measurements, followed by the presentation of the new proposed correlation and, finally, the comparison of the experimental data with the correlations found in the open literature and with the new developed correlation.

<sup>2</sup> The horizontal Schubring's experimental data of the liquid film thickness were measured in bottom ( $\delta_{bottom}$ ), side ( $\delta_{side}$ ) and top ( $\delta_{top}$ ) of the test section, consequently a mean film thickness has been used to correlate these data. This magnitude is defined as.

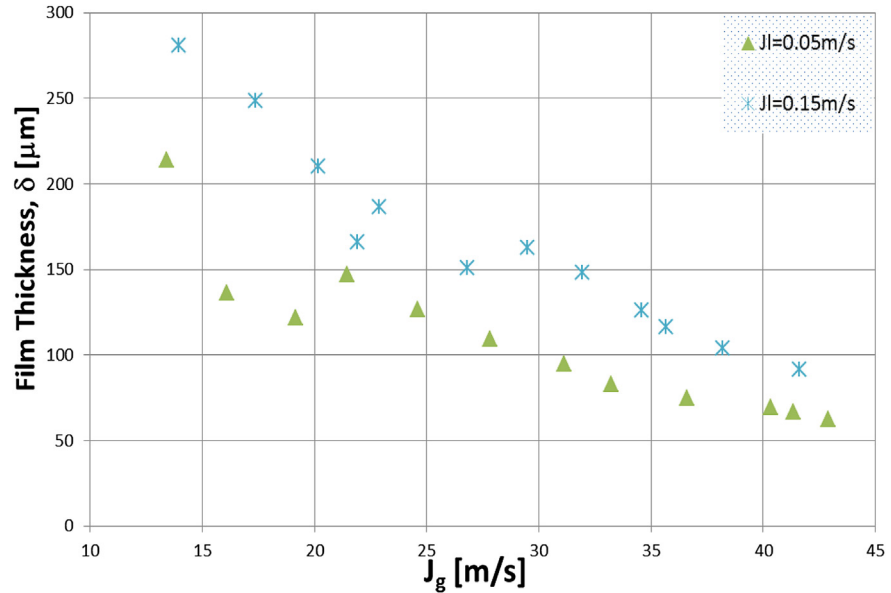


**Fig. 12.** Alamu's experimental liquid film thickness data vs. superficial gas velocity (vertical upward flow,  $D = 0.019$  m,  $P = 1.4$  bars,  $T_{\text{ambient}}$ , working fluids: air–water–glycerin) with constant liquid velocity.

### 5.1.1. Initial analysis of liquid film thickness from the experimental data

First, we present a previous analysis of the experimental data in order to have a general view of the liquid film thickness behavior in each experimental series. Figs. 10 and 11 display the

liquid film thickness versus the gas superficial velocity with constant liquid velocity for Schubring's vertical data series, and the liquid film thickness versus the liquid superficial velocity with constant gas velocity for Schubring's horizontal data, respectively. From both figures, it can be seen that, as gas

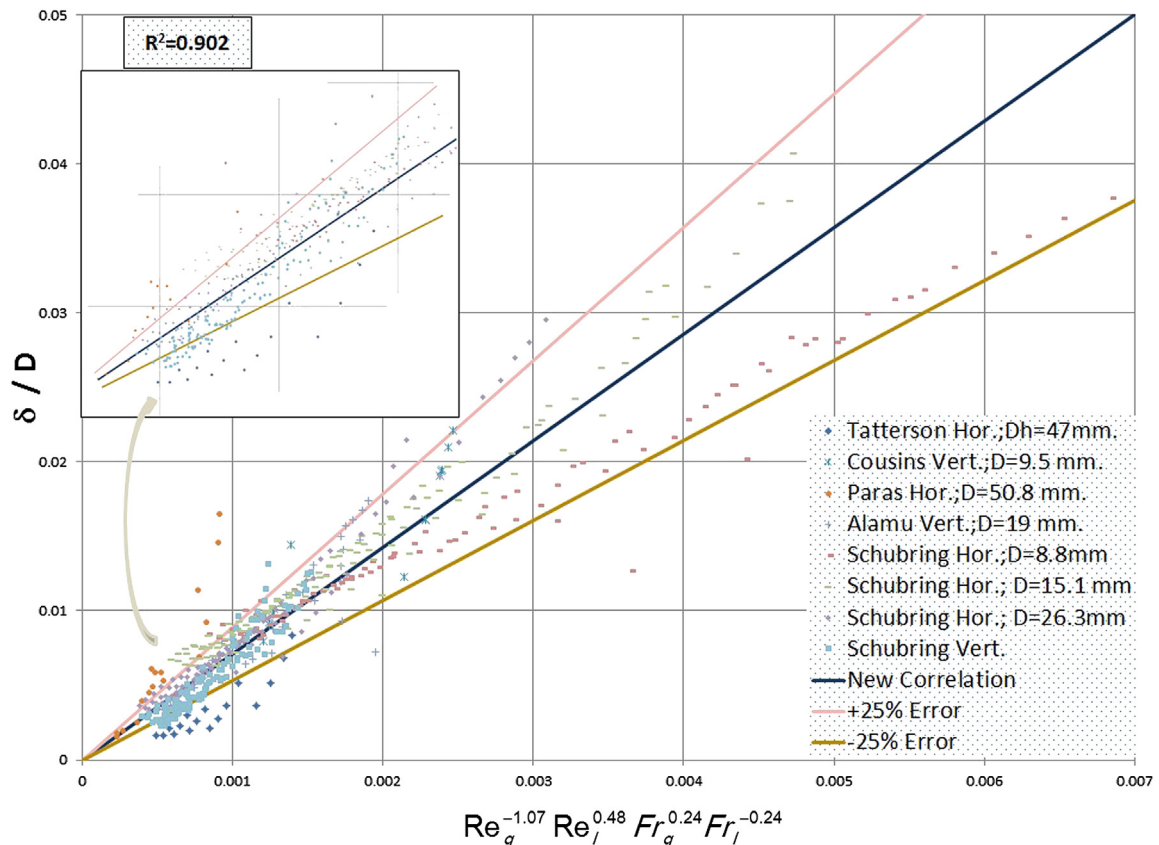


**Fig. 13.** Comparison of liquid film thickness experimental data with the new correlation developed in the present study.

velocity increases, a decrease in the liquid film thickness is produced and vice versa. Whereas for liquid superficial velocity, there is the opposite trend, as liquid superficial velocity increases (increase in total liquid mass flow) liquid film thickness increases too; although this tendency becomes less noticeable as the gas velocity increases, until it becomes practically constant for high gas velocities. This trend can be seen very clearly in Fig. 11, which shows that, for low superficial gas velocities, the trend lines are ranked in a decreasing thickness order. While with the increase of gas velocity this trend breaks, being liquid film thicknesses greater for higher gas velocities. For example, the lowest thicknesses are measured experimentally for gas velocities of 60–52 m/s, whereas for higher gas velocities (89–79, 79–70 and 70–58 m/s) the liquid film thicknesses are greater. The same trends that have been explained previously are observed for Alamu's experimental data, in this case for a mixture of water and glycerin, as can be seen in Fig. 12.

### 5.1.2. New correlation of liquid film thickness

From the experimental data discussed above, a large number of adjustments have been made in order to correlate the liquid layer film thickness with the physical properties and conditions under which the experiments have been carried out. In particular, we have taken as variables for the adjustment the corresponding dimensionless numbers, in order to obtain more general relationships. For the determination of these dimensionless numbers have been needed, as mentioned above, the physical properties of the working fluids and the conditions of the experiments, namely gas and liquid superficial velocities, densities and dynamic viscosities for both fluids, and surface tension of the liquid phase (obtained from the experimental pressure and temperature conditions and from the working fluids composition). Thus, finally, the new correlation obtained is

$$\frac{\delta}{D} = 7.165 \cdot Re_g^{-1.07} Re_l^{0.48} \left( \frac{Fr_g}{Fr_l} \right)^{0.24} \quad (86)$$

where, for the gas and liquid phases, the Reynolds and Froude numbers are defined by Eqs. (14), (18), (19) and (21), respectively, in which these dimensionless numbers are defined in terms of superficial velocities.

The fitting of the new correlation with the experimental data shown in the previous section is presented in Fig. 13. As can be seen in the figure, the new correlation produces a reasonable fitting for all experimental data, as they almost collapse to the correlation's line. In fact, almost all of them are located between the error lines of  $\pm 25\%$ , with a value for the Pearson product-moment correlation coefficient of  $R^2 = 0.902$ .

### 5.1.3. Comparison of liquid film thickness correlations with experimental data

This section is devoted to compare the results obtained with the available correlations, including the new correlation presented earlier, Eq. (86), with the experimental data (for more details see Section 2.2.1 and Table 3). The next figures, from Figs. 14–17, show the variation of the liquid film thickness with the superficial liquid velocity, maintaining constant the gas superficial velocity and vice versa. In all figures, in order to calculate the liquid film thickness, the liquid Reynolds number has been employed in terms of the

**Table 3**  
Summary of correlations for the liquid film thickness.

Reference	Correlation
Ambrosini (Rodriguez, 2009)	$\delta_l^+ = \frac{\rho_l \delta u_l^*}{\mu_l} = \begin{cases} 0.34 Re_{lf}^{0.6} & Re_{lf} \leq 1000 \\ 0.0512 Re_{lf}^{0.875} & Re_{lf} > 1000 \end{cases} \quad (12)$ $u_l^* = \sqrt{\frac{\tau_i}{\rho_l}}$ $\tau_i = \frac{1}{2} f_{gi} \rho_g (u_g - u_{lf})^2$
Fukano (Fukano and Furukawa, 1998)	$\frac{\delta}{D} = 0.0594 \exp(-0.34 Fr_g^{0.25} Re_l^{0.19} x^{*0.6}) \quad (13)$ $x^* = \frac{J_g \rho_g}{J_g \rho_g + J_l \rho_l}$
Hori (Fukano and Furukawa, 1998)	$\frac{\delta}{D} = 0.905 Re_g^{-1.45} Re_l^{0.90} Fr_g^{0.93} Fr_l^{-0.68} \left( \frac{\mu_l}{\mu_{l,ref}} \right)^{1.06} \quad (20)$
Henstock (Henstock and Hanratty, 1976)	<i>Vertical flows</i> $\frac{\delta}{D} = \frac{6.59 F}{(1 + 1400 F)^{0.5}} \quad (22)$  <i>Horizontal flows</i> $\frac{\delta}{D} = \frac{6.59 F}{(1 + 850 F)^{0.5}} \quad (23)$ $F = \frac{1}{\sqrt{2}} \frac{Re_l^{0.5} \mu_l \rho_g^{0.5}}{Re_g^{0.4} Re_g^{0.9} \mu_g \rho_l^{0.5}}$
Tatterson (Tatterson et al., 1977)	<i>Vertical flows</i> $\frac{\delta}{D} = \frac{6.59 F}{(1 + 1400 F)^{0.5}} \quad (22)$  <i>Horizontal flows</i> $\frac{\delta}{D} = \frac{6.59 F}{(1 + 850 F)^{0.5}} \quad (23)$ $F = \frac{\gamma(Re_{lf}) \mu_l \rho_g^{0.5}}{Re_g^{0.9} \mu_g \rho_l^{0.5}}$
Roberts (Roberts et al., 1997)	$\gamma(Re_{lf}) = \left[ (0.707 Re_{lf}^{0.5})^{2.5} + (0.0379 Re_{lf}^{0.9})^{2.5} \right]^{0.4} \quad (25)$ $\delta = 846 \frac{D}{D_{ref}} \frac{Re_{lf}^{0.44}}{Re_g^{0.59}} \quad (27)$
Okawa (Okawa et al., 2002)	$\delta = \frac{1}{4} \sqrt{\frac{f_{wg} \rho_l}{f_{gi} \rho_g}} \frac{J_{lf} D}{J_g} \quad (28)$
Ishii (Ishii and Grolmes, 1975)	$\delta = 0.347 Re_{lf}^{2/3} \sqrt{\frac{\rho_l}{\tau_i}} \frac{\mu_l}{\rho_l} \quad (29)$
New correlation	$\frac{\delta}{D} = 7.165 \cdot Re_g^{-1.07} Re_l^{0.48} \left( \frac{Fr_g}{Fr_l} \right)^{0.24} \quad (86)$

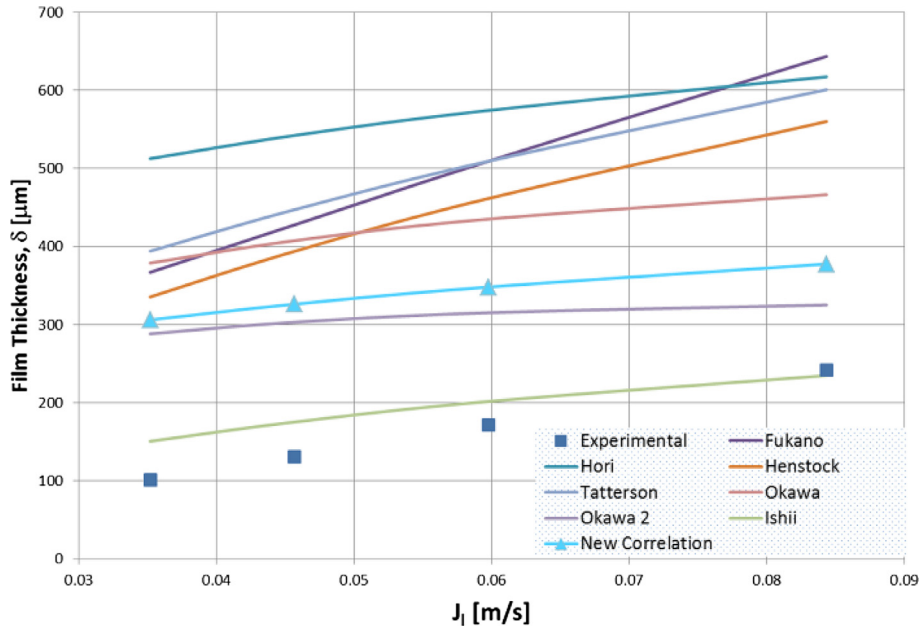


**Fig. 14.** Comparison of liquid film thickness vs. superficial liquid velocity of Tatterson's data (horizontal flow, channel  $0.305 \times 0.025$  m,  $P$  and  $T$  ambient,  $J_g \cong 35$  m/s) for the available correlations.

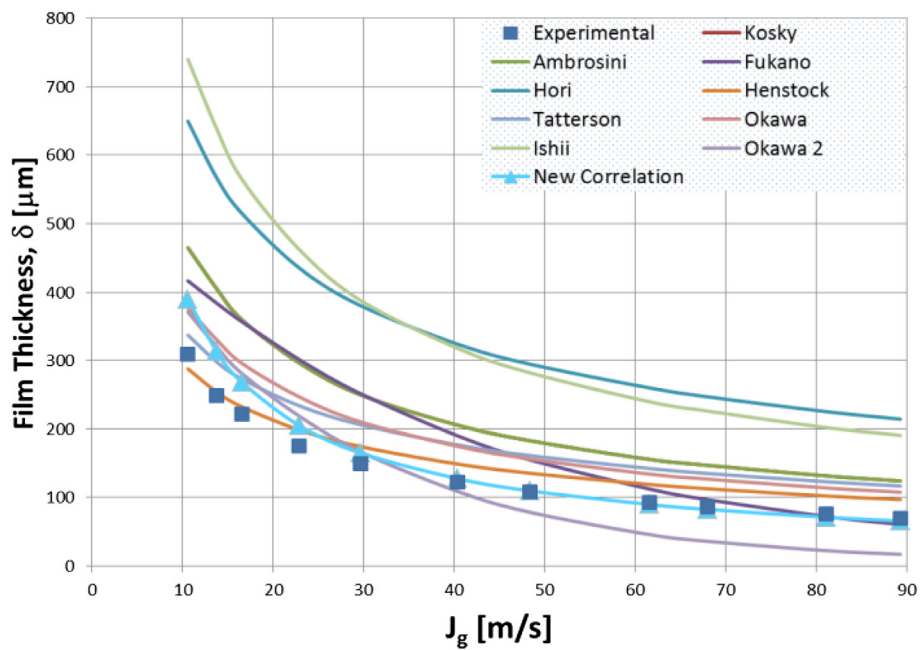


**Fig. 15.** Comparison of liquid film thickness vs. superficial gas velocity of Schubring's horizontal data (horizontal flow,  $D = 0.0088$  m,  $P$  and  $T$  ambient,  $J_l = 0.192$  m/s) for the available correlations.

superficial liquid velocity. This has been done this way to have more simple equations, due to the fact that the entrained fraction,  $E$ , is not usually available in the experimental measurements. But to see the difference between the two possibilities, the Okawa's expression has been presented in both forms. For the estimation of  $E$ , the article of Cioncolini and Thome (2010) and the Mantilla's (2008) thesis can be consulted.

Fig. 14 displays the comparison of Tatterson's experimental measurements with the values predicted by several correlations studied, and by the new one proposed correlation. As can be seen,

Ishii's correlation gives the best results, followed by Okawa's,<sup>3</sup> and the new proposed correlation, being the remaining correlations further from the experimental measurements. We have presented

<sup>3</sup> The difference between the called Okawa and Okawa 2 correlations during all the present section is that Okawa's correlation is obtained from Eq. (28), but without taking into consideration the entrained fraction, that is  $E = 0$ ; whereas Okawa 2 has been obtained using directly Eq. (28), in which  $E$  must be estimated from a correlation.

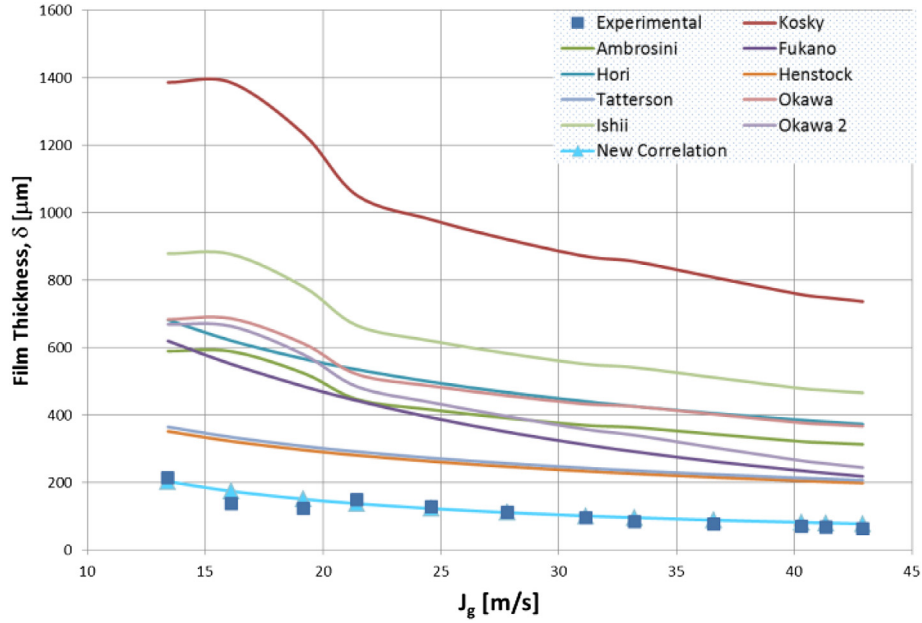


**Fig. 16.** Comparison of liquid film thickness vs. superficial gas velocity of Alamu's data (vertical flow,  $D = 0.019$  m,  $P = 1.4$  bar and  $T_{\text{ambient}}$ ,  $J_l = 0.05$  m/s, air–water–glycerin) for the available correlations.

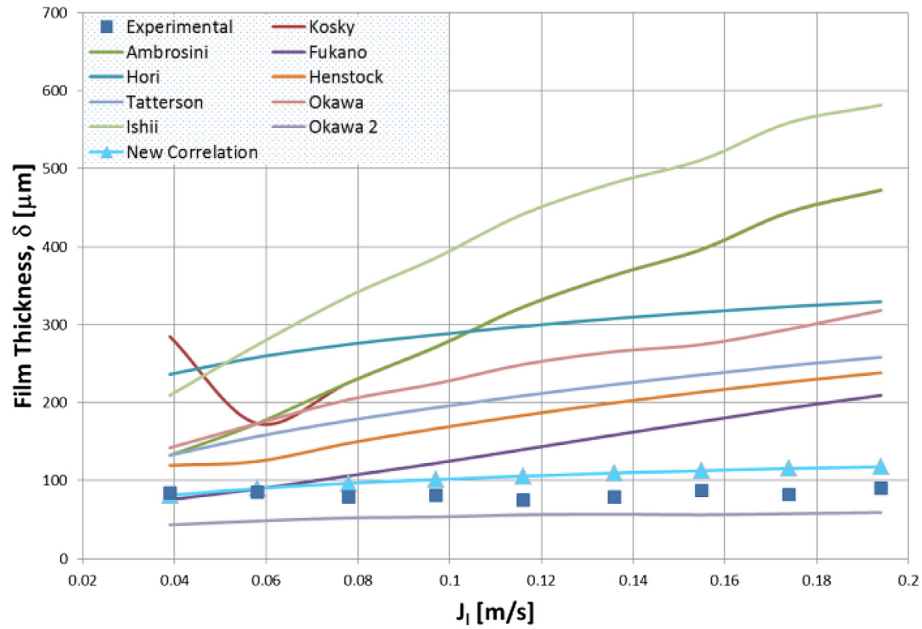


**Fig. 17.** Comparison of liquid film thickness vs. superficial liquid velocity of Schubring's vertical data (vertical upward flow,  $D = 0.0234$  m,  $P$  and  $T_{\text{ambient}}$ ,  $J_g \approx 71$  m/s) for the available correlations.

this figure first to indicate that the new correlation is not the best fit for this experimental series, as well as some cases of Paras's series. But for the newest experimental measurements of Alamu (made with a mixture of water and glycerin in standpipe) and for all Schubring's series (made for both horizontal and vertical flow in the latter case for 3 different sizes of pipe with about 500 experimental values), the adjustments are really good, as can be seen in Figs. 15–17. In these last cases, the Kosky's and Ambrosini's correlations presented earlier, which are the ones that best fitted Tatterson's series, present significant deviations. We must conclude by saying that the new correlation provides better results than the other ones studied, although in certain specific cases some of the other correlations provide more accurate results.

## 5.2. Wave celerity

In the present section, we have analyzed the following experimental data series<sup>4</sup>: Mantilla's (2008), Schubring (2008) and Alamu (2010). The experimental conditions of Schubring's and Alamu's measurements have been introduced in the previous section. Whereas Mantilla's experimental conditions were the following: all measurements were conducted in horizontal pipes, the air–water

<sup>4</sup> Mantilla's experimental data include measurements of wave celerity below the onset of entrainment, which have not been used for the realization of the settings, since this point marks the beginning of droplet entrainment processes.

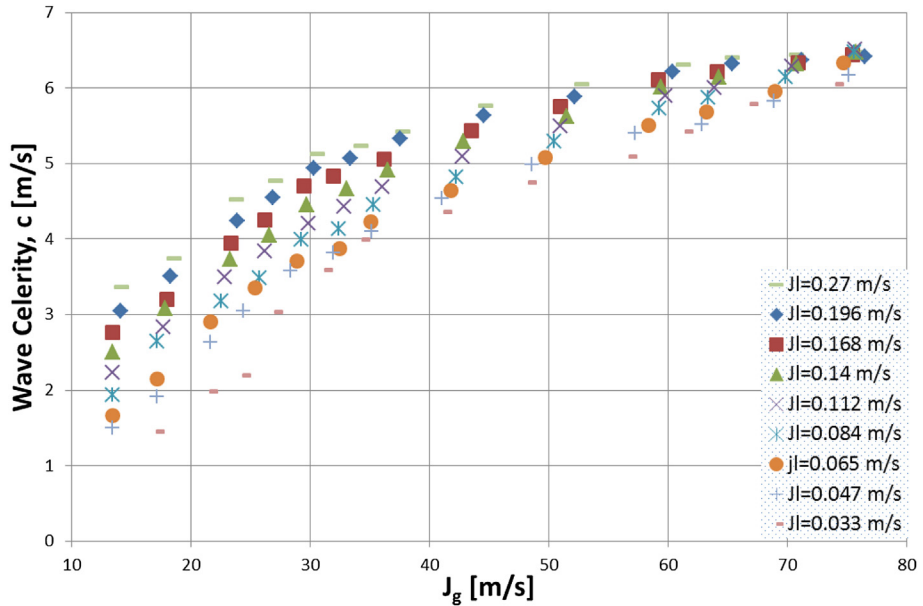


**Fig. 18.** Schubring's experimental wave celerity data vs. superficial gas velocity (horizontal flow,  $D = 0.0151$  m,  $P$  and  $T$  ambient, working fluids: air–water) with constant liquid velocity.

series were made in pipes of 4.86 and 15.3 cm of inner diameters, while the air–water–butanol and air–water–glycerin–salt were made only for the 4.86 cm pipe. The temperature in all cases was ambient conditions, whereas pressure was ambient for air–water series in the 15.3 cm pipe, and 2 bars for the rest of measurements.

This section is organized in the same way as the previous one. First, an initial analysis of the available experimental measurements, followed by the presentation of the new proposed correlation and, finally, the comparison of the experimental data with the correlations found in the open literature, and with the new developed correlation.

#### 5.2.1. Initial analysis of wave celerity from the experimental data

In order to have a general view of the wave celerity behavior in each experimental series, a previous analysis has been done. In Fig. 18 it is shown the wave celerity versus the gas superficial velocity with constant liquid velocity for a 1.51 cm diameter pipe under horizontal flow conditions (Schubring's experimental measurements). From the figure, it can be seen that, as gas velocity increases, an increase in the wave celerity is produced, and the wave celerity increases when the liquid superficial velocity increases too. But only for low gas velocities, because this increase with liquid velocity becomes smaller, until it disappears for higher

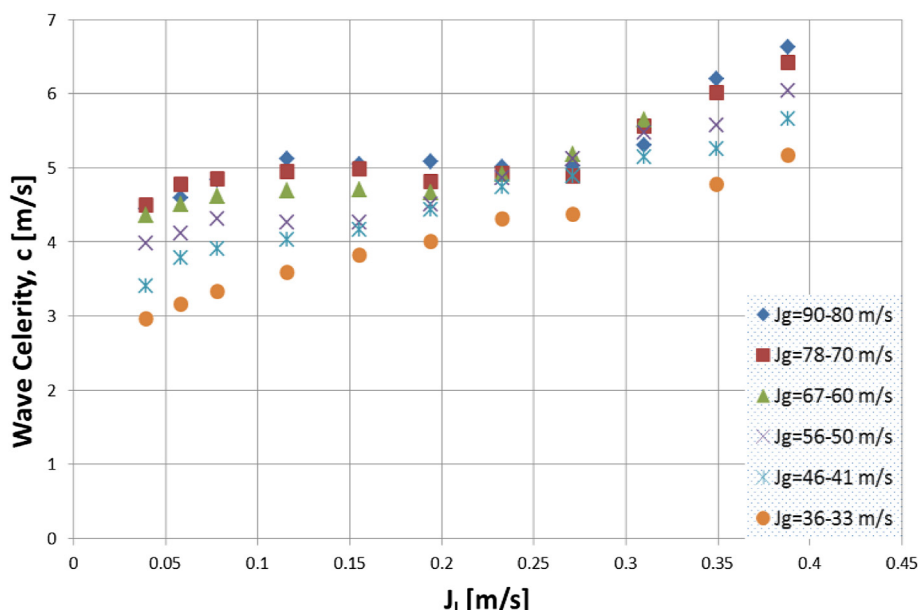


**Fig. 19.** Schubring's experimental wave celerity data vs. superficial liquid velocity (vertical upward flow,  $D = 0.0234$  m,  $P$  and  $T$  ambient, working fluids: air–water) with constant gas velocity.

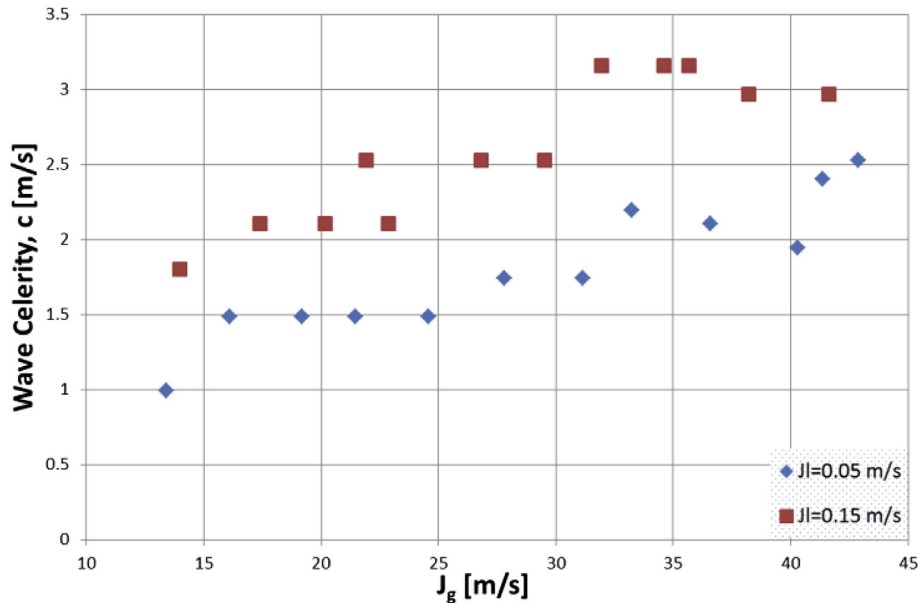


**Fig. 20.** Alamu's experimental wave celerity data vs. superficial gas velocity (vertical upward flow,  $D = 0.019 \text{ m}$ ,  $P = 1.4 \text{ bars}$ ,  $T_{\text{ambient}}$ , working fluids: air–water–glycerin) with constant liquid velocity.

gas velocities. Whereas for vertical upward data (Schubring's experimental measurements presented in Fig. 19), it can be seen that, in general, there is an increasing trend of wave celerity for both gas and liquid superficial velocities. While, for intermediate values of liquid velocity, in some cases the mentioned increase does not occur, but stabilizes. For mixtures of water with glycerin and water with butanol, being for vertical and horizontal flows, respectively, it is noted that wave celerity increases with gas and liquid superficial velocities, see Figs. 20 and 21. The same trend is observed for all the analyzed experimental series. Therefore, it can be said that this is the general trend of wave celerity with gas and liquid superficial velocities.

### 5.2.2. New correlation of wave celerity

From the experimental data discussed above, a large number of adjustments have been made in order to correlate wave celerity with physical properties and conditions at which the experiments have been carried out. In particular, we have taken as variables for the adjustment the corresponding dimensionless numbers, in order to obtain more general relationships. For the determination of these dimensionless numbers have been needed, as mentioned above, the physical properties of the working fluids and the conditions of the experiments, namely gas and liquid superficial velocities, densities and dynamic viscosities for both fluids, and surface tension of the liquid phase (obtained from the experimental

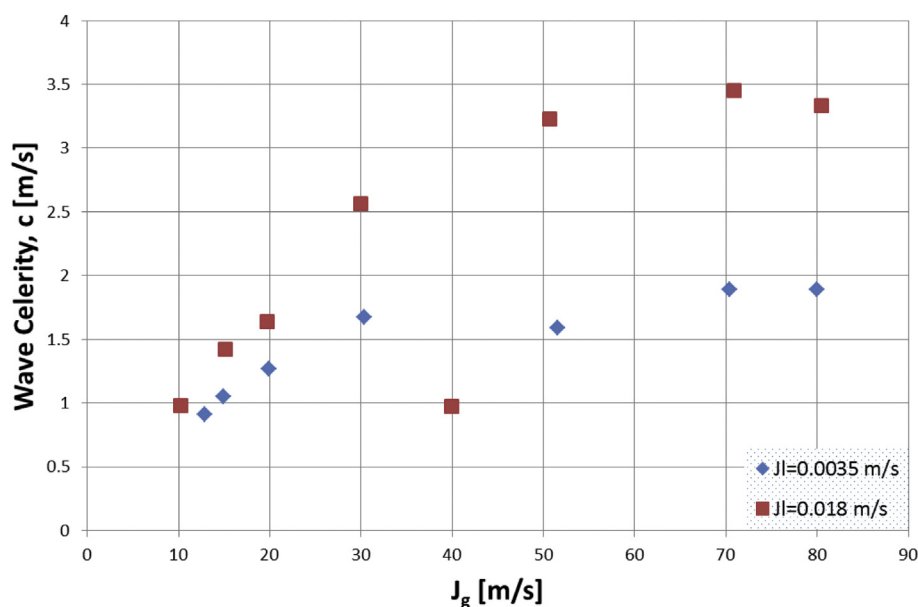


**Fig. 21.** Mantilla's experimental wave celerity data vs. gas superficial velocity (horizontal flow,  $D = 0.0486 \text{ m}$ ,  $P = 2 \text{ bars}$ ,  $T_{\text{ambient}}$ , working fluids: air–water–butanol), effect of liquid velocity with constant liquid velocity.

pressure and temperature conditions and composition of the working fluids). Regarding wave celerity normalization, various possibilities have been studied, such as: dividing by gas superficial velocity, the square root of gas and liquid velocities product, etc., but the final choice is the one shown below. Then, the new correlation is

$$\frac{c}{\sqrt{\rho_g J_g + \sqrt{\rho_l J_l}}} = Re_g^{-0.38} Re_l^{0.16} C_W^{-0.13} \quad (87)$$

where the gas and liquid Reynolds numbers are defined in terms of the gas and liquid superficial velocities, respectively, Eqs. (19) and (18). The expression for the surface tension factor is the one defined originally by Ishii, Eq. (37).

The fitting of the proposed new correlation with the experimental data shown in the previous section is presented in Fig. 22. As can be seen in the figure, the new correlation produces a reasonable fitting of all experimental data, as they collapse almost all data to the correlation's line. In fact, almost all of them are located between the error lines of  $\pm 25\%$ , with a value for the Pearson product-moment correlation coefficient of  $R^2 = 0.885$ .

### 5.2.3. Comparison of wave celerity correlations with experimental data

This section is devoted to compare the results for wave celerity obtained with the available correlations, including the new correlation presented earlier Eq. (87), with the experimental data (for more details see Section 2.2.4 and Table 4). The next figures, from Figs. 23–26, show the variation of the wave celerity with the superficial liquid velocity, maintaining constant the gas superficial velocity and vice versa.

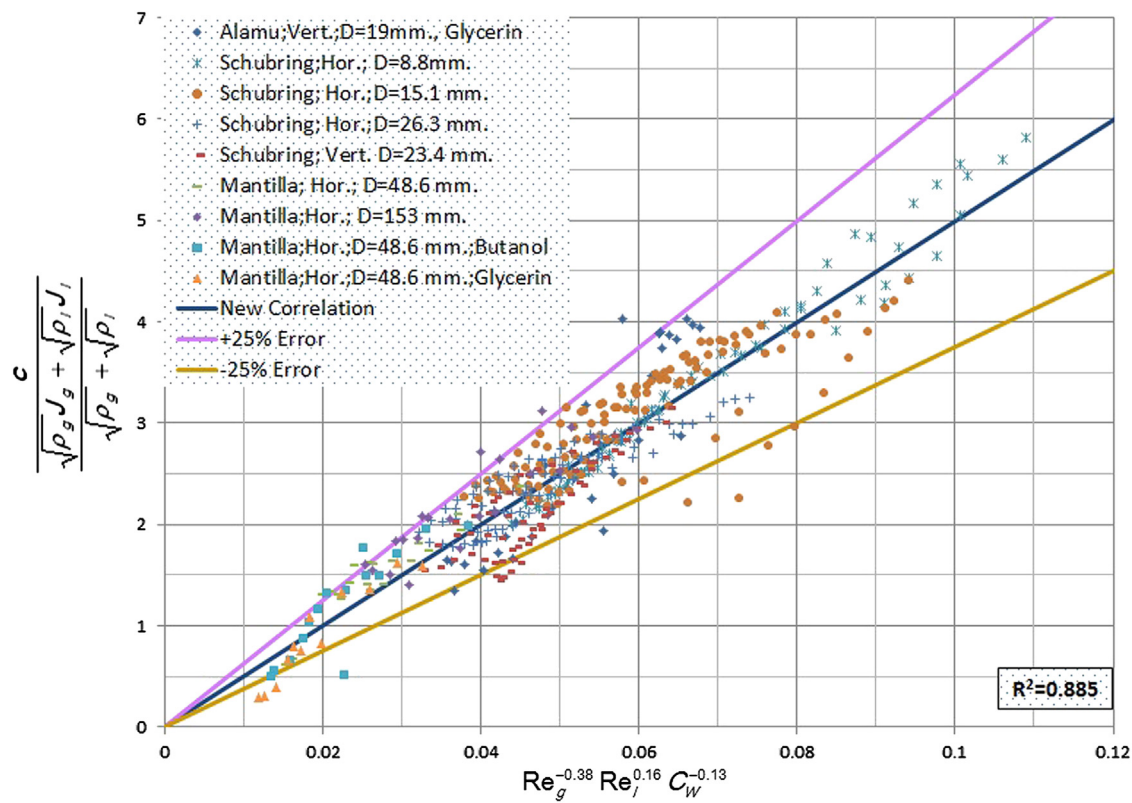


**Fig. 22.** Comparison of experimental data of wave celerity with the new correlation developed in the present study.

**Table 4**  
Summary of correlations for the wave celerity.

Reference	Correlation
Kumar (Mantilla, 2008)	$c = \frac{\psi J_g + J_l}{1+\psi}$ Eq. (45) $\psi = 5.5 \sqrt{\frac{\rho_g}{\rho_l}} \left( \frac{Re_l}{Re_g} \right)^{0.25}$
Marmottant (Belt et al., 2010)	$c = \frac{\sqrt{\rho_g J_g + \sqrt{\rho_l J_l}}}{\sqrt{\rho_g + \sqrt{\rho_l}}} \text{ Eq. (51)}$
Schubring (Schubring and Shedd, 2009)	$c = 0.41 \frac{J_g}{\sqrt{\chi}} Re_g^{-0.25}$ Eq. (52) $x = \frac{m_g}{m_g + m_l}$
Al-Sarkhi (Al-Sarkhi et al., 2012)	Horizontal $\frac{c}{J_l} = 2.379 \cdot X^{-0.9}$ Eq. (54) Inclination 10–20° $\frac{c}{J_l} = 2.323 \cdot X^{-0.94}$ Eq. (55) Inclination 45–90° $\frac{c}{J_l} = 1.942 \cdot X^{-0.91}$ Eq. (56)
New correlation	$X = \sqrt{\frac{\rho_l J_g}{\rho_g J_g}}$ $\frac{c}{\sqrt{\rho_g J_g + \sqrt{\rho_l J_l}}} = Re_g^{-0.38} Re_l^{0.16} C_W^{-0.13}$ Eq. (87)

Fig. 23 displays the comparison of Schubring's experimental measurements in a horizontal pipe with inner diameter of 1.51 cm, compared with the predictions done by several correlations. As can be seen, the correlation proposed in this work give the best results; only for low superficial gas velocities the Kumar's correlation is closer to the experimental data. The results obtained for Schubring's vertical upward data are displayed in Fig. 24, but in this case, the figure shows the variation of wave celerity as function of superficial liquid velocity. As in the previous figure, the correlation proposed in the present article gives quite good results, especially for low superficial liquid velocities, while for higher values the correlation of Kumar gives the best results. For Alamu's

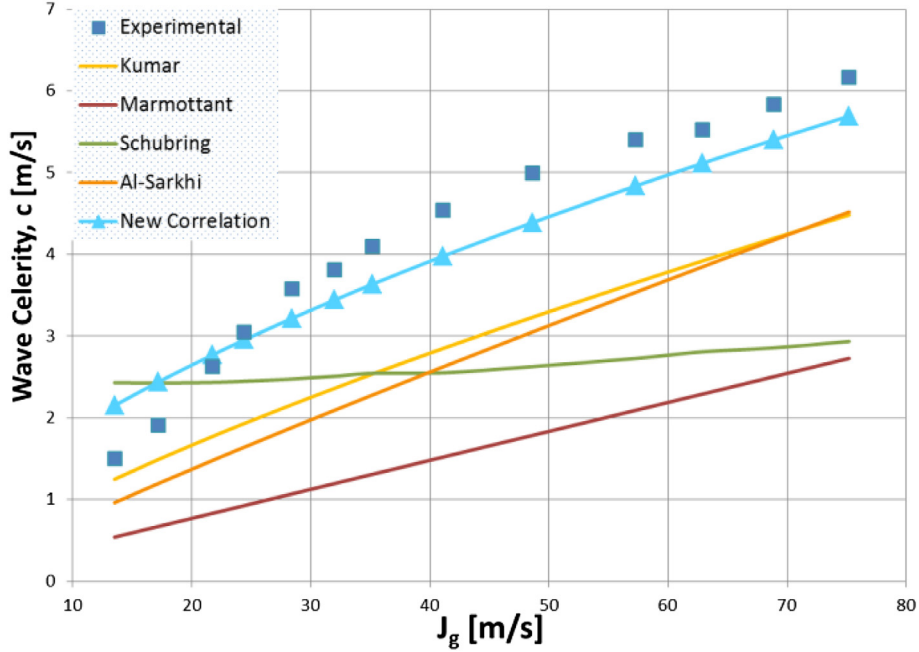


**Fig. 23.** Comparison of wave celerity vs. superficial gas velocity of Schubring's horizontal data (horizontal flow,  $D = 0.0151$  m,  $P$  and  $T$  ambient,  $J_l = 0.065$  m/s) for the available correlations.

measurements, Fig. 25, with vertical upward conditions and a mixture of water and glycerin, the situation is quite similar to the previous figure. In this case, the new correlation proposed here gives somewhat higher values than the experimental ones, whereas the expression of Kumar gives slightly lower values, although the predictions of the equation developed here is slightly closer. Finally, Fig. 26 displays the results for Mantilla's data of a water-butanol mixture. In this case the correlations that are closer to the experimental measurements are also the Kumar and the one

developed in this paper. We must conclude by saying that the new correlation provides better results than other correlations studied, although Kumar's expression presents good results too, being closer to the experimental measurements.

### 5.3. Wave frequency

The experimental series analyzed in order to study the frequency of the waves that appear on the gas–liquid surface are the

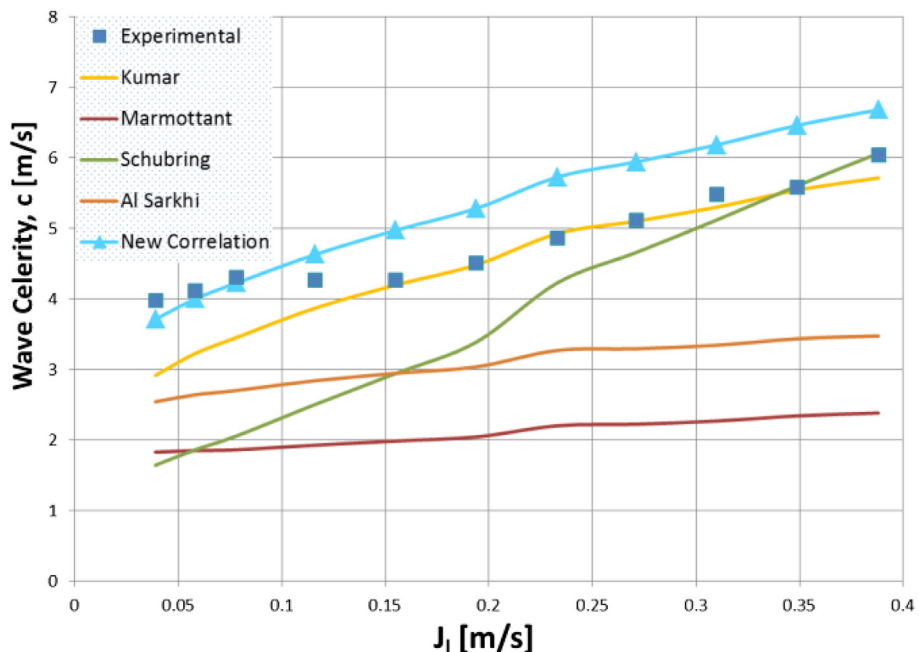


**Fig. 24.** Comparison of wave celerity vs. superficial liquid velocity of Schubring's data (vertical upward flow,  $D = 0.0234$  m,  $P$  and  $T$  ambient, working fluids: air–water,  $J_g \approx 56$ – $60$  m/s) for the available correlations.

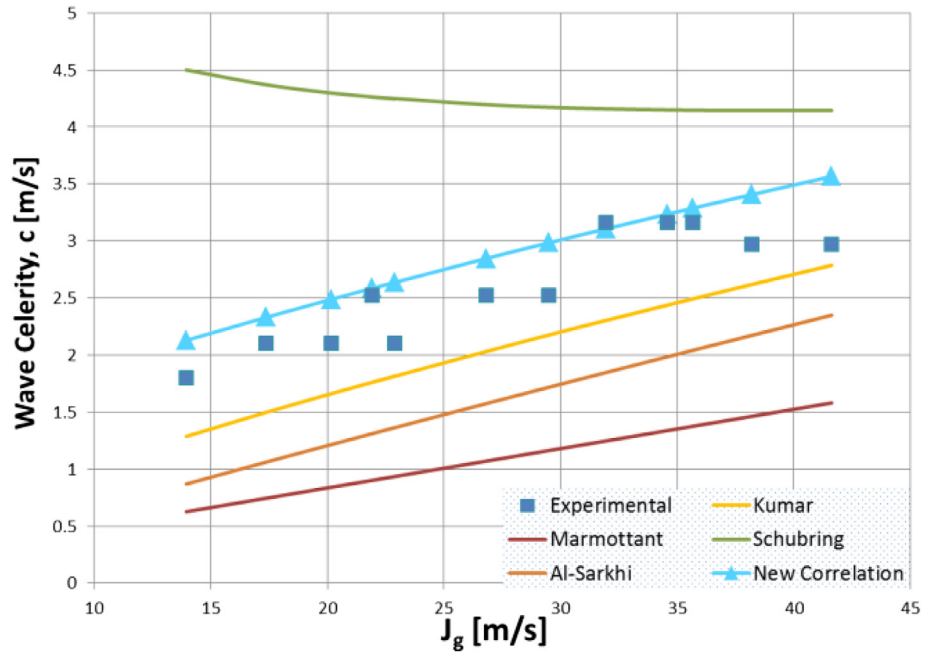


**Fig. 25.** Comparison of wave celerity vs. superficial gas velocity of Alamu's data (vertical upward flow,  $D = 0.019$  m,  $P = 1.4$  bars,  $T$  ambient, working fluids: air–water–glycerin,  $J_l = 0.15$  m/s) for the available correlations.

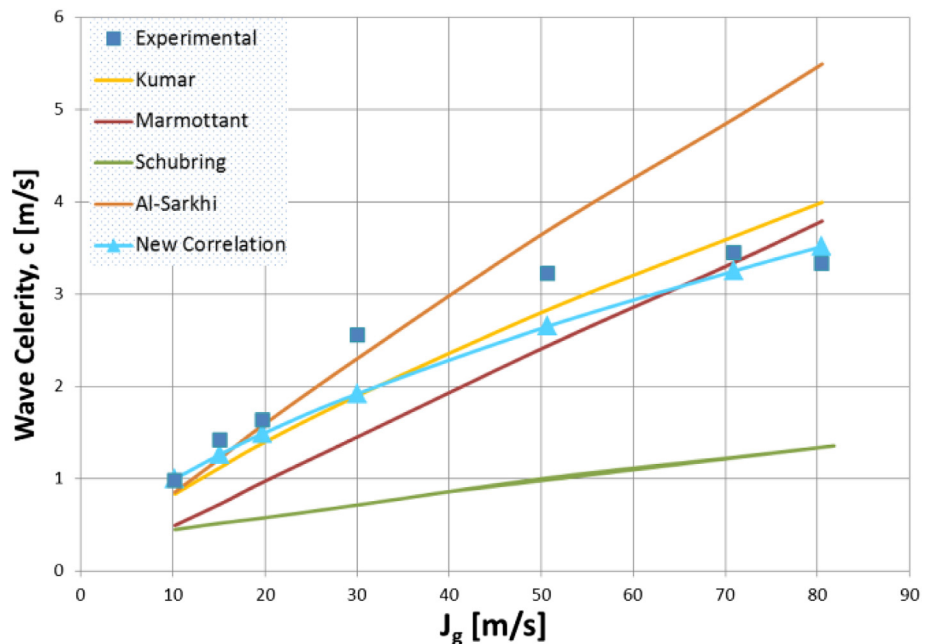


**Fig. 26.** Comparison of Wave celerity vs. superficial gas velocity of Mantilla's data (horizontal flow,  $D = 0.0486$  m,  $P = 2$  bars,  $T$  ambient, working fluids: air–water–butanol,  $J_l = 0.018$  m/s) for the available correlations.

same ones that have been used to correlate the wave celerity in the previous section, that is to say<sup>5</sup>: Mantilla (2008), Schubring (2008) and Alamu (2010) measurement series.

This section is organized in the same way as the two previous sections. First, an initial analysis of the available experimental measurements, followed by the presentation of the new proposed

correlation and, finally, the comparison of the experimental data with the correlations found in the open literature, and with the new developed correlation.

### 5.3.1. Initial analysis of wave frequency from the experimental data

In order to have a general view of the wave frequency behavior in each experimental series, a previous analysis has been done. In Fig. 27 it is plotted the wave frequency versus the liquid superficial velocity with constant gas velocity for horizontal flow conditions with the 2.63 cm diameter pipe of Schubring's data. From the

<sup>5</sup> As in the wave celerity, Mantilla's experimental data include measurements of wave frequency below the onset of entrainment, which have not been used for the realization of the settings.

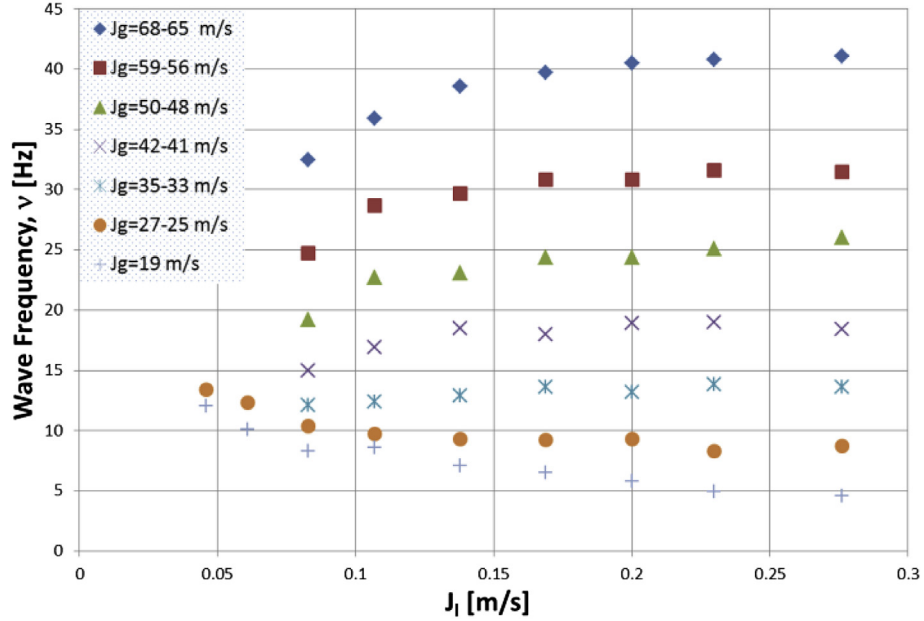


**Fig. 27.** Schubring's experimental wave frequency data vs. superficial liquid velocity (horizontal flow,  $D = 0.0263$  m,  $P$  and  $T$  ambient, working fluids: air–water) with “constant” gas velocity.

figure, it can be deduced that, for higher values of gas superficial velocity; as liquid velocity increases, an increase in the wave frequency is produced. However, the slope of this increase reduces progressively until, at about 30 m/s, is almost flat, and below this value, the wave frequency decreases with the increase of liquid superficial velocity. As can seen in the figure, the wave frequency also increases with gas superficial velocity at constant liquid superficial velocities. Whereas for vertical upward data (Schubring's experimental measurements presented in Fig. 28), it can be seen that, in general, there is an increasing trend of wave frequency with gas superficial velocity, but the slope of this increase is smaller for

bigger superficial liquid velocities. However, at low values of gas and liquid superficial velocities there are lower frequencies, whereas higher gas superficial velocities and lower liquid superficial velocities produce higher waves frequencies. For mixtures of water with butanol in horizontal flow conditions (Mantilla's series), there is the opposite tendency, as explained in the previous lines, see Fig. 29. While Alamu's measurements, Fig. 30, which used as working liquid a mixture of water-glycerin in vertical flow conditions, there is a lower wave frequency with lower gas and liquid superficial velocities, having a steeper slope for the higher value of the liquid superficial velocity. These last two statements must be

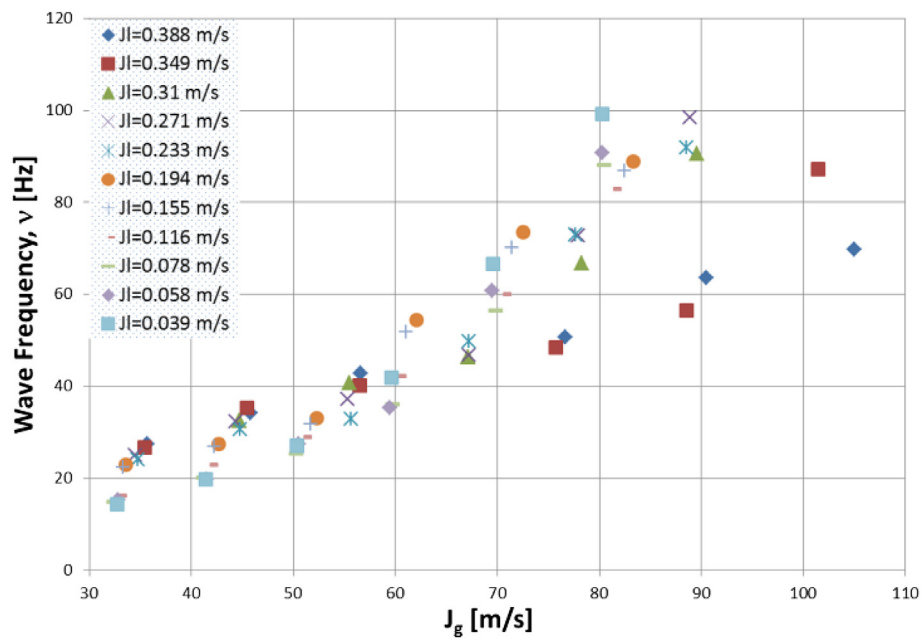


**Fig. 28.** Schubring's experimental wave celerity data vs. superficial gas velocity (vertical upward flow,  $D = 0.0234$  m,  $P$  and  $T$  ambient, working fluids: air–water) with constant liquid velocity.

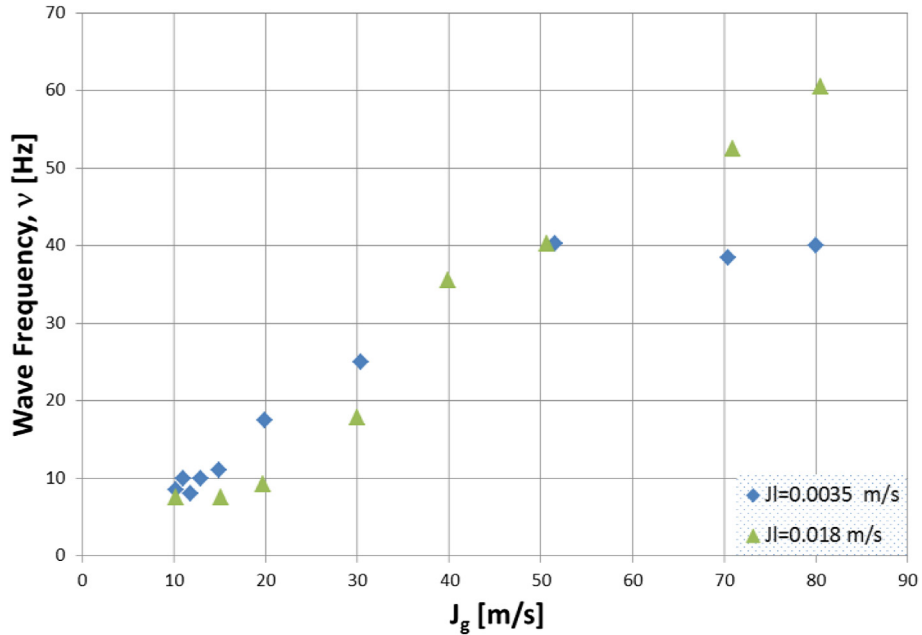


**Fig. 29.** Mantilla's experimental wave celerity data vs. gas superficial velocity (horizontal flow,  $D = 0.0486 \text{ m}$ ,  $P = 2 \text{ bars}$ ,  $T_{\text{ambient}}$ , working fluids: air–water–butanol), effect of liquid velocity with constant liquid velocity.

made with appropriate caution, as only two different liquid rates are available.

The same trend is observed for all the analyzed experimental series. Therefore, it can be said that there is a general increasing trend of wave frequency with gas and liquid superficial velocities, except for low gas superficial velocities in Schubring's measurements, made in horizontal flow conditions, in which the tendency is in the opposite direction.

### 5.3.2. New correlation for the wave frequency

From the experimental data discussed above, a large number of adjustments have been made in order to correlate wave

frequency with physical properties and conditions in which the experiments have been carried out. In particular, we have taken as variables for the adjustment the corresponding dimensionless numbers, in order to obtain more general relationships. For the determination of these dimensionless numbers, has been needed, as mentioned above, the physical properties of the working fluids and the conditions of the experiments, namely gas and liquid superficial velocities, densities and dynamic viscosities for both fluids, and surface tension of the liquid phase (obtained from the experimental pressure and temperature conditions, and from the working fluids composition). Then, the new correlation proposed is

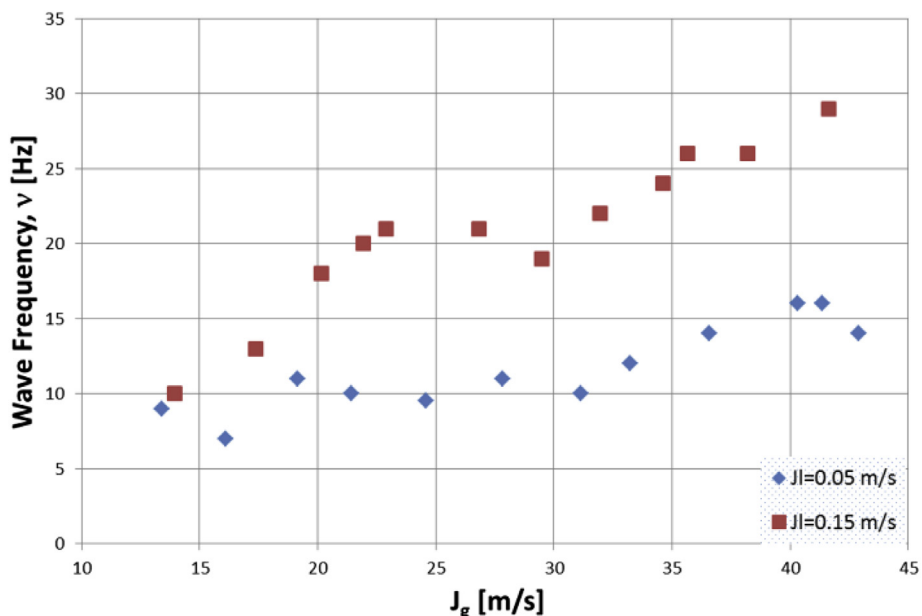


**Fig. 30.** Alamu's experimental wave celerity data vs. superficial gas velocity (vertical upward flow,  $D = 0.019 \text{ m}$ ,  $P = 1.4 \text{ bars}$ ,  $T_{\text{ambient}}$ , working fluids: air–water–glycerin) with constant liquid velocity.

$$St_{gl} = Re_g^{0.53} Re_l^{-0.48} Eo^{0.27} \left( \frac{\rho_g}{\rho_l} \right)^{0.14} C_W^{0.68} \quad (88)$$

where  $St_{gl}$  is the gas–liquid Strouhal number, which has been defined in the same way that liquid Strouhal number, Eq. (59), and gas Strouhal number, Eq. (62),  $St_{gl}$  is defined as

$$St_{gl} = \frac{vD}{\sqrt{J_g J_l}} \quad (89)$$

where the gas and liquid Reynolds numbers are defined in terms of the gas and liquid superficial velocities, respectively, Eqs. (19) and (18). The Eötvös number is defined by Eq. (63). The expression of the surface tension factor is the same one as originally defined by Ishii, Eq. (37).

The fitting of the proposed new correlation with the experimental data shown in the previous section is presented in Fig. 31. As can be seen in the figure, the new correlation does not produce a quite good fitting of the experimental data, but it collapses almost all data between the error lines of  $\pm 50\%$ , with a value for the Pearson product–moment correlation coefficient of  $R^2 = 0.683$ .

### 5.3.3. Comparison of wave frequency correlations with experimental data

This section is devoted to compare the experimental results for the wave frequency with the results obtained with the available correlations, including the new correlation presented earlier Eq. (88) (for more details see Section 2.2.5 and Table 5).

As it is shown in Figs. 32–36, which display the experimental measurements and results of the correlations studied, the expression which gives better predictions of the experimental data is the correlation proposed in the present article.

Generally speaking, we must say that there is an upward trend in wave frequency with both liquid and gas superficial velocities, which is well reproduced by the proposed correlation. This increase takes place for all working fluids and in all conditions studied, only in some specific cases of Schubring's measures for low gas velocities

**Table 5**  
Summary of correlations for the wave frequency.

Reference	Correlation
Azzopardi (Azzopardi, 2006)	$St_l = 0.25X^{-1.2}$ Eq. (58) $St_l = \frac{vD}{J_l}$
Sekoguchi (Sawant et al., 2008b)	$St_g = \frac{vD}{J_g} = f_1(Eo)f_2(Re_l, Fr_g)$ Eq. (62) $Eo = \frac{gD^2(\rho_l - \rho_g)}{\sigma}$ $f_1(Eo) = Eo^{-0.5}[0.5\ln(Eo) - 0.47]$ $f_2(Re_l, Fr_g) = 0.0076\ln\left(\frac{Re_l}{Fr_g}\right) - 0.051$
Sawant (Sawant et al., 2008b)	$St_g = 0.086Re_l^{0.27} \left( \frac{\rho_l}{\rho_g} \right)^{-0.64}$ Eq. (65)
New correlation	$St_{gl} = Re_g^{0.53} Re_l^{-0.48} Eo^{0.27} \left( \frac{\rho_g}{\rho_l} \right)^{0.14} C_W^{0.68}$ Eq. (88) $St_{gl} = \frac{vD}{\sqrt{J_g J_l}}$ $C_W = \begin{cases} 0.028N_\mu^{-4/5} & \text{for } N_\mu \leq 1/150.25 \\ 1 & \text{for } N_\mu > 1/150.25 \end{cases}$ $N_\mu = \frac{\mu_l}{\left( \rho_l \sigma \sqrt{\frac{\sigma}{g \Delta \rho}} \right)^{1/2}}$

there is a decrease in wave frequency with increasing superficial liquid velocity, as noted above, see Fig. 27. We must highlight the wide range of variation that presents this magnitude, from low values in the range of 3–5 m/s for pipe 15.3 cm in diameter, Fig. 34, to values hovering around 100 m/s for some Schubring's series at high gas velocities, Fig. 33. Also we must mention the good agreement obtained with the proposed correlation for working liquids different to water, concretely mixtures of water with butanol, and water with glycerin, Figs. 35 and 36. In all cases, the correlation proposed here provides a suitable outcome, note that Azzopardi's correlation also gives good estimations for most cases, except for the measurements performed in the larger diameter pipes (Mantilla's measurements series in a pipe diameter of 15.3 cm). Finally, we must conclude that the correlation proposed here shows a better performance than the other expressions found in the literature.

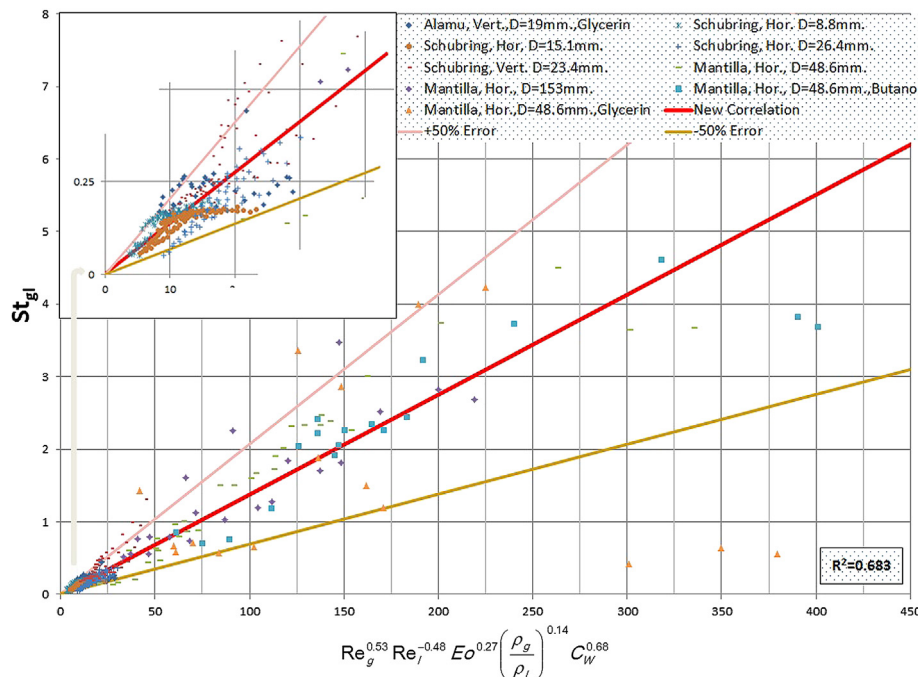


**Fig. 31.** Comparison of experimental data of wave frequency with the new correlation developed in the present study.

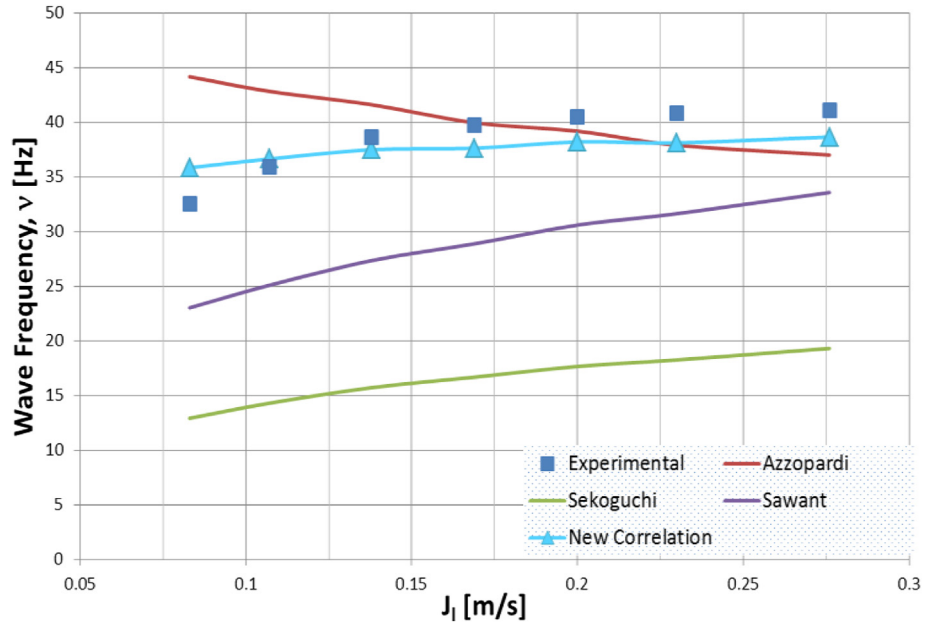


**Fig. 32.** Comparison of wave frequency vs. superficial liquid velocity of Schubring's horizontal data (horizontal flow,  $D = 0.0263$  m,  $P$  and  $T$  ambient,  $J_g \cong 66$  m/s) for the available correlations.

## 6. Conclusions

An in-depth characterization of liquid and liquid–gas interface is mandatory for a thorough understanding of annular two-phase flow. An extensive review of phenomena, together with a collection and analysis of data found in the open literature for key variables defining the liquid–gas interface, have been described in the present paper.

Liquid–gas interface shows a wavy structure that very much depends on the liquid and gas flow rates magnitudes. A thorough review of their properties (i.e., amplitude and frequency) has been done in previous sections.

In the present work, a number of insights into key two-phase flow variables have been drawn, either from analyses reported in the literature or from new analysis that have yielded new correlations for those variables:

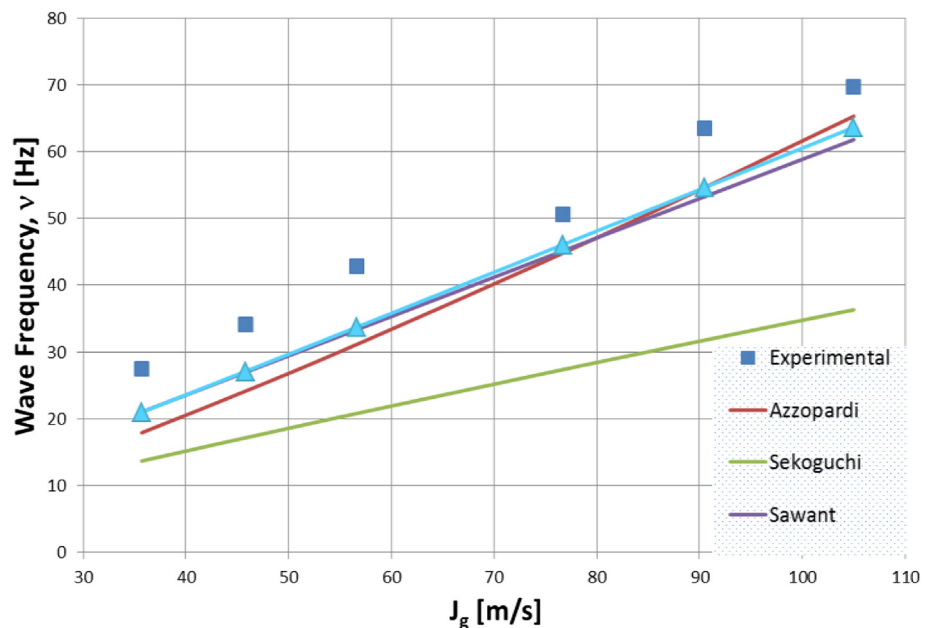


**Fig. 33.** Comparison of wave frequency vs. superficial gas velocity of Schubring's data (vertical upward flow,  $D = 0.0234$  m,  $P$  and  $T$  ambient, working fluids: air–water,  $J_l = 0.388$  m/s) for the available correlations.

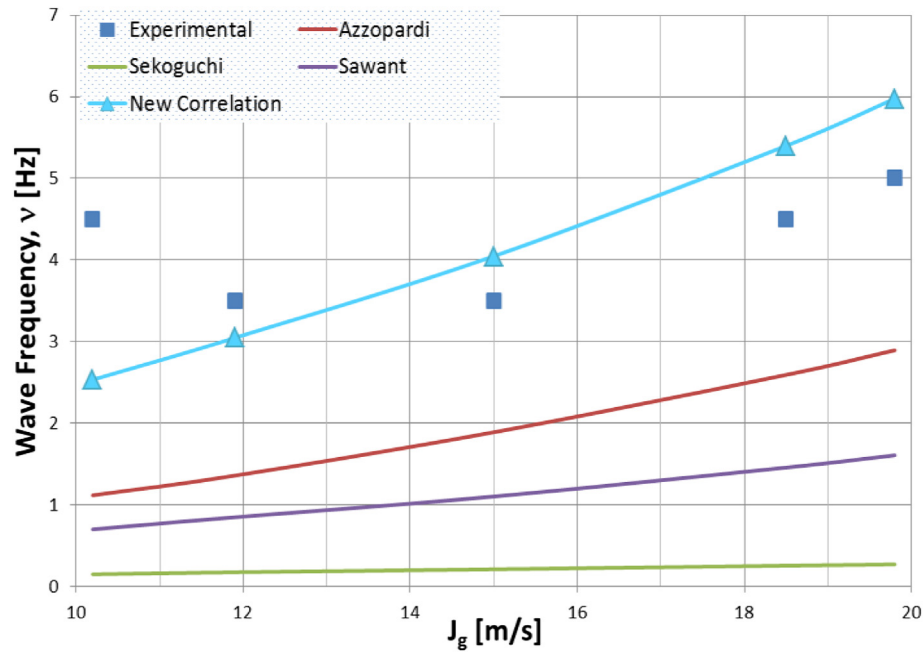


**Fig. 34.** Comparison of wave frequency vs. superficial gas velocity of Mantilla's horizontal data (horizontal flow,  $D = 0.153$  m,  $P$  and  $T$  ambient,  $J_l = 0.018$  m/s) for the available correlations.

### 6.1. Liquid film thickness

Liquid film thickness decreases with increasing superficial gas velocity, although this decrease becomes smaller for higher gas velocities. Liquid film thickness increases with superficial liquid velocity.

A new correlation to obtain the liquid film thickness as function of dimensionless numbers has been developed. Liquid film thickness has been made non-dimensional with pipe diameter and correlated with the dimensionless numbers which better fit the experimental results. In this case, these

dimensionless numbers have been Reynolds and Froude numbers of gas and liquid phases. This new correlation has been compared to the available ones found in the open literature and an improvement in the estimations of this magnitude has been achieved.

### 6.2. Wave celerity

Wave celerity increases when increasing superficial gas velocity, although this increase becomes slightly smaller for higher gas velocities.

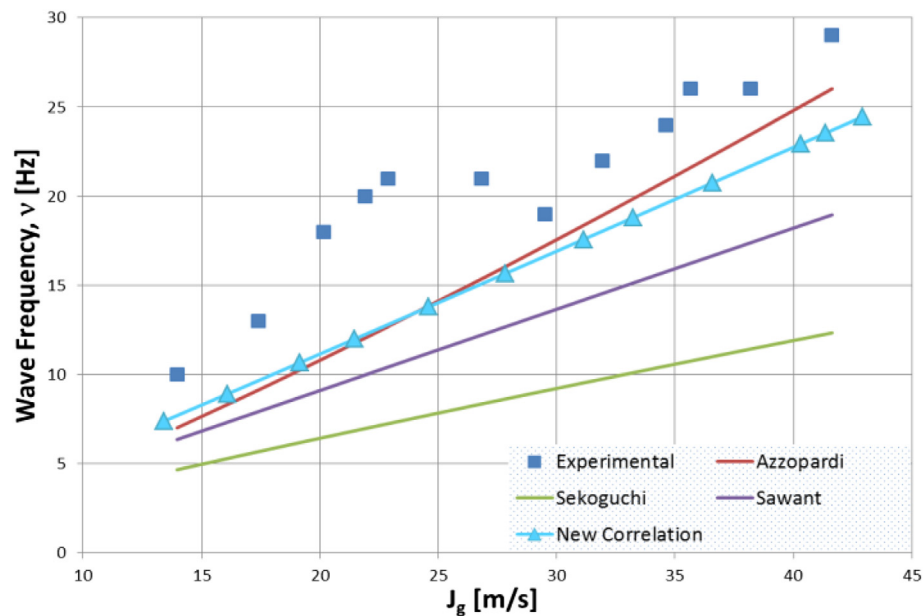


**Fig. 35.** Comparison of wave frequency vs. superficial gas velocity of Alamu's data (vertical upward flow,  $D = 0.019$  m,  $P = 1.4$  bars,  $T$  ambient, working fluids: air–water–glycerin,  $J_l = 0.15$  m/s) for the available correlations.

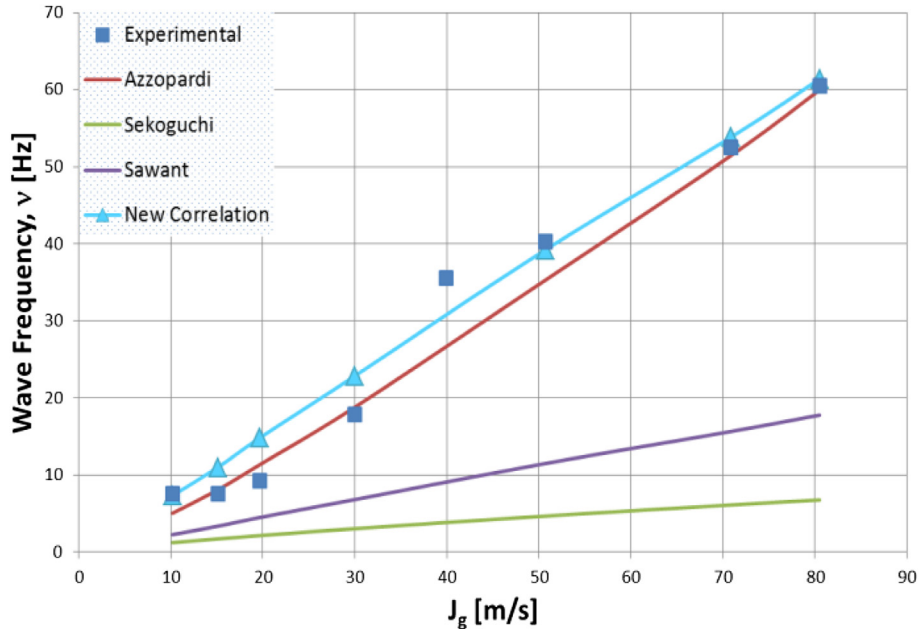


**Fig. 36.** Comparison of wave frequency vs. superficial gas velocity of Mantilla's data (horizontal flow,  $D = 0.0486$  m,  $P = 2$  bars,  $T_{\text{ambient}}$ , working fluids: air–water–butanol,  $J_l = 0.018$  m/s) for the available correlations.

Wave celerity increases with the decrease of liquid superficial velocity, although this increase is not large.

A new correlation to obtain the wave celerity as a function of dimensionless numbers has been developed. Wave celerity has been made non-dimensional with gas and liquid velocities averaged with their densities and correlated with the dimensionless numbers which better fit the experimental results. In this case, the dimensionless numbers used have been gas and liquid Reynolds numbers and the viscosity number. This correlation has been compared to the available ones found in the open literature and an improvement in the estimations of this magnitude has been achieved.

### 6.3. Wave frequency

Wave frequency is strongly influenced by the gas superficial velocity. An increase in this magnitude is produced with the increase of gas superficial velocity, although this increase becomes smaller for higher gas velocities.

Wave frequency is strongly influenced by liquid superficial velocity. This magnitude increases with the liquid superficial velocity, although for high gas superficial velocities, wave frequency remains constant.

A new correlation to obtain the wave frequency as a function of dimensionless numbers has been developed. We have obtained the wave frequency from the Strouhal number, but defined in terms of the geometric mean of gas and liquid superficial velocities. The Strouhal number has been correlated with the dimensionless numbers which better fit the experimental results. In this case, the dimensionless numbers used have been gas and liquid Reynolds numbers, the viscosity number and the density ratio. This correlation has been compared to the available expression found in the open literature, and an improvement in the estimation of this magnitude has been achieved.

Regarding the entrainment processes, when a gas is flowing over a liquid film, the gas–liquid interface may become unstable depending on the magnitude of the gas and liquid velocities. On one hand, there is the onset of entrainment Reynolds number,

$Re_{\text{ffOE}}$  below which no entrainment is possible. Nevertheless, when looking through literature one may find numbers ranging from 80 to 500 for air–water systems in horizontal or vertical orientations. The most usual is 160, as proposed by Ishii and Grolmes. On the other hand, even if  $Re_l > Re_{\text{ffOE}}$  condition is met, gas velocity should be greater than a given threshold for entrainment to take place. Several expressions to estimate this entrainment inception velocity (i.e., Kutateladze criterion, Ishii and Grolmes model, Sawant model, etc.) have been found and collected in this paper.

We must finalize this work by emphasizing the development of new correlations for the key variables of annular two-phase flow, which produces a noticeable improvement, compared with those found in the open literature. Also, we must highlight that a coming paper on behavior and characterization of entrained droplets resulting from liquid–gas interaction at high gas velocity is currently under preparation, and it will properly close-up the two-phase annular flow study.

### Acknowledgements

The authors are indebted to the plan of I + D support of the project REMODERN ENE2010-21368-C02-01/CON.

### References

- Alamu, M.B., 2010. Investigation of Periodic Structures in Gas–Liquid Flow. PhD. thesis. University of Nottingham.
- Aleksenko, S., Antipin, V., Cherdantsev, A., Kharlamov, S., Markovich, D., 2009. Two-wave structure of liquid film and wave interrelation in annular gas–liquid flow with and without entrainment. *Phys. Fluids* 21 (1), 061701.
- Aleksenko, S., Antipin, V., Cherdantsev, A., Kharlamov, S., Markovich, D., 2008. Investigation of waves interaction in annular gas–liquid flow using high-speed fluorescent visualization technique. *Microgravity Sci. Technol.* 20 (1), 271.
- Alipchenkov, V.M., Nigmatulin, R.I., Soloviev, S.L., Stonik, O.G., Zaichik, L.I., Zeigarnik, Y.A., 2004. A three-fluid model to two-phase dispersed-annular flow. *Int. J. Heat. Mass Transfer* 47, 5323–5338.
- Al-Sarkhi, A., Sarica, C., Magrini, K., 2012. Inclination effects of wave characteristics in annular gas–liquid flows. *AIChE J.* 58, 1018–1029.
- Andreussi, P., Asali, J.C., Hanratty, T.J., 1985. Initiation of roll waves in gas–liquid flows. *AIChE J.* 31 (1), 119–126.
- Arnold, C.R., Hewitt, G.F., 1967. Further developments in the photography of two phase gas–liquid flow. *J. Photogr. Sci.* 15, 97–114.

- Asali, J.C., Hanratty, T.J., 1993. Ripples generated on a liquid film at high gas velocities. *Int. J. Multiphase Flow* 19 (2), 229–243.
- Asali, J.C., Hanratty, T.J., Andreussi, P., 1985. Interfacial drag and film height for vertical annular flow. *Am. Inst. Chem. Eng. J.* 31 (6), 895–902.
- Azzopardi, B.J., 1983. Mechanisms of Entrainment in Annular Two-phase Flow. UKAEA Report AERE-11068.
- Azzopardi, B.J., 1997. Drops in annular two-phase flow. *Int. J. Multiphase Flow* 23, 1–53.
- Azzopardi, B.J., 2006. Gas-Liquid Flows. Begell House Inc., New York.
- Belt, R.J., Van't Westende, J.M.C., Prasser, H.M., Portela, L.M., 2010. Time and spatially resolved measurements of interfacial waves in vertical annular flow. *Int. J. Multiphase Flow* 36, 570–587.
- Brodkey, R.S., 1967. The Phenomena of Fluid Motions. Addison-Wesley, p. 112.
- Chandrasekhar, S., 1981. Hydrodynamic and Hydromagnetic Stability. Oxford University Press.
- Chung, H.S., Murgatroyd, W., 1965. Studies of the mechanism of roll wave formation on thin liquid films. In: Symposium On Two-phase Flow, Paper A2, Exeter, UK vol. 2.
- Cioncolini, A., Thome, J.R., 2010. Prediction of the entrained liquid fraction in vertical annular gas–liquid two-phase flow. *Int. J. Multiphase Flow* 36, 293–302.
- Cooper, K.D., Hewitt, G.F., Pinchin, B., 1964. Photography of two-phase gas–liquid Flow. *J. Photogr. Sci.* 12, 269.
- Cousins, L.B., Denton, W.H., Hewitt, G.F., 1965. Liquid mass transfer in annular two-phase flow. In: Symposium on Two Phase Flow, Exeter, Engand.
- Crowe, C.T., 2006. Multiphase Flow Handbook (Mechanical Engineering). CRC Press, Taylor&Francis Group.
- Dallman, J.C., 1978. Investigation of Separated Flow Model in Annular Gas–liquid Two-phase Flows. Ph.D. thesis. University of Illinois, Urbana.
- Epstein, M., 1990. Theory od scrubbing of volatile fission product vapour containing gas jet in a water pool. In: ANS Winter Meeting November 11–16 1990, Washington DC, pp. 21–32.
- Flores, A.G., Crowe, K.E., Griffith, P., 1995. Gas-phase secondary flow in horizontal, stratified and annular two-phase flow. *Int. J. Multiph. Flow* 21 (2), 207–221.
- Fukano, T., Furukawa, T., 1998. Prediction of the effects of liquid viscosity on interfacial shear stress and frictional pressure drop in vertical upward Gas–Liquid annular flow. *Int. J. Multiphase Flow* 24 (4), 587–603.
- Hall-Taylor, N.S., Hewitt, G.F., Lacey, P.M.C., 1963. The motion and frequency of large disturbance waves in annular two-phase flow of air–water mixtures. *Chem. Eng. Sci.* 18, 537–552.
- Han, H., Zhu, Z., Gabriel, K., 2006. A study on the effect of gas flow rate on the wave characteristics in two-phase gas–liquid annular flow. *Nucl. Eng. Des.* 236, 2580–2588.
- Hanratty, T.J., Engen, M., 1957. Interaction between a turbulent air stream and a moving water surface. *AIChE J.* 3, 299.
- Hanratty, T.J., Hershman, A., 1961. Initiation of roll waves. *Am. Inst. Chem. Eng. J.* 7, 488.
- Henstock, W.H., Hanratty, T.J., 1976. The interfacial drag and the height of the wall layer in annular flows. *AIChE J.* 22 (6), 990–1000.
- Hewitt, G.F., Govan, A.H., 1990. Phenomena and prediction in annular two-phase flow advances in gas-liquid flows. In: American Society of Mechanical Engineers, Winter Meeting, pp. 41–56.
- Hewitt, G.F., Hall-Taylor, N.S., 1970. Annular Two-phase Flow. Pergamon Press, Oxford, pp. 136–139.
- Hewitt, G.F., Lovegrove, P.C., 1969. Frequency and Velocity Measurements of Disturbance Waves in Annular Two-phase Flow. UKAEA Report, AERE-R4304.
- Hills, J.H., 1997. The critical liquid flow rates for wave and droplet formation in annular gas–liquid flow. In: Exp. Heat Transfer Fluid Mech. Thermodyn., pp. 1241–1247. ETS 2.
- Hinze, 1955. Fundamentals of the hydrodynamic mechanism of splitting in dispersion process. *AIChE J.* 1.
- Hollowach, M.J., Hochreiter, L.E., Cheung, F.B., 2002. A model for droplet entrainment in heated annular flow. *Int. J. Heat. Fluid Flow* 23, 807–822.
- Hughmark, G.A., 1973. Film thickness, entrainment and pressure drop in upward annular and dispersed flow. *AIChE J.* 19, 1062–1065.
- Ishii, M., Grolmes, M.A., 1975. Inception criteria for droplet entrainment in two-phase concurrent film flow. *AIChE J.* 21, 308–318.
- Jacowitz, L.A., Brodkey, R.S., 1964. An analysis of geometry and pressure drop for the horizontal annular two-phase flow of water and air in the entrance region of a pipe. *Chem. Eng. Sci.* 19 (4), 261–274.
- Jiao, B., Qiu, L., Gan, Z., 2009. Liquid film dryout model for predicting critical heat flux in annular two-phase flow. *J. Zhejiang Univ. Sci.* 10 (3), 398–417.
- Lamb, H., 1975. Hydrodynamics, sixth ed. Cambridge University Press.
- Laurinat, J.E., 1982. Studies of the Effects of Pipe Size on Horizontal Annular Two-phase Flows. Ph.D. thesis. University of Illinois, Urbana.
- Levich, V.G., 1962. Physicochemical Hydrodynamics. Prentice-Hall, Englewood Cliffs, NJ.
- Levy, S., 1999. Two-phase Flow in Complex Systems. John Wiley & Sons Inc.
- Lopez de Bertodano, M.A., Assad, A., Beus, S.G., 1998. Entrainment Rate for Droplets in the Ripple-annular Regime for Small Vertical Tubes. Bettis Atomic Power Laboratory. Document DE-AC11-93PN38195.
- MacGillivray, R., 2004. Gravity and Gas Density Effects on Annular Flow Average Film Thickness and Frictional Pressure Drop. Ph.D. thesis. University of Saskatchewan, Saskatoon, Canada.
- Mantilla, I., 2008. Mechanistic Modeling of Liquid Entrainment in Gas in Horizontal Pipes. Ph.D. thesis. University of Tulsa.
- Martin, C.J., 1983. Annular Two Phase Flow. Ph.D. thesis. Oxford University, U.K.
- Ohba, K., Nagae, K., 1993. Characteristics and behavior of the interfacial wave on the liquid film in a vertically upward air-water two-phase annular flow. *Nucl. Eng. Des.* 141 (1–2), 17–25.
- Okawa, T., Kitahara, T., Yoshida, K., Matsumoto, T., Kataoka, I., 2002. New entrainment rate correlation in annular two-phase flow applicable to wide range of flow condition. *Int. J. Heat. Mass Transfer* 45, 87–98.
- Okawa, T., Kotani, A., Kataoka, I., Naito, M., 2003. Prediction of critical heat flux in annular flows using a film flow model. *J. Nucl. Sci. Technol.* 40, 388–396.
- Omebere-Iyari, Azzopardi, B.J., 2007. A study of flow pattern for gas/liquid flow in small diameter tubes. *Chem. Eng. Res. Des.* 85, 180–192.
- Owen, D.G., Hewitt, G.F., 1987. An improved annular two-phase flow model. In: Proceedings of the Third International Conference on Multiphase Flow, the Hague, the Netherlands.
- Pan, L., Hanratty, T.J., 2002a. Correlation of entrainment for annular flow in vertical pipes. *Int. J. Multiphase Flow* 32, 363–384.
- Pan, L., Hanratty, T.J., 2002b. Correlation of entrainment for annular flow in horizontal pipes. *Int. J. Multiphase Flow* 32, 385–408.
- Paras, S.V., Karabelas, A.J., 1991. Properties of the liquid layer in horizontal annular flow. *Int. J. Multiphase Flow* 17 (4), 439–454.
- Roberts, P.A., Azzopardi, B.J., Hibberd, S., 1997. The split of horizontal annular flow at a T-Junction. *J. Chem. Eng. Sci.* 52 (20), 3441–3453.
- Rodriguez, J.M., 2009. Numerical Simulation of Two-phase Annular Flow. Ph.D. thesis. Rensselaer Polytechnic Institute of New York.
- Sawant, P., Ishii, M., Mori, M., 2008a. Droplet entrainment correlation in vertical upward co-current annular two-phase flow. *Nucl. Eng. Des.* 238, 1342–1352.
- Sawant, P., Ishii, M., Hazuku, T., Takamasa, T., Mori, M., 2008b. Properties of disturbance waves in vertical annular two-phase flow. *Nucl. Eng. Des.* 238, 3528–3541.
- Sawant, P., Ishii, M., Mori, M., 2009. Prediction of amount of entrained droplets in vertical annular two-phase flow. *Int. J. Heat. Fluid Flow* 30, 715–728.
- Schadel, S.A., 1988. Atomization and Deposition Rates in Vertical Annular Two-phase Flow. Ph.D. thesis. University of Illinois, Urbana-Champaign, Urbana, Illinois, USA.
- Schubring, D., Shedd, T.A., 2008. Wave behavior in horizontal annular air–water flow. *Int. J. Multiphase Flow* 34, 636–646.
- Schubring, D., Shedd, T.A., 2009. Critical friction factor modeling of horizontal annular base film thickness. *Int. J. Multiphase Flow* 35, 389–397.
- Schubring, D., 2008. Behavior Interrelationships in Annular Flow. PhD thesis. University of Wisconsin-Madison.
- Sekoguchi, K., Takeishi, M., Ishimatsu, T., 1985. Interfacial structure in vertical upward annular flow. *Phys. Chem. Hydrodyn.* 6, 239–255.
- Tatterson, D.F., Dallman, J.C., Hanratty, T.J., 1977. Drop sizes in annular gas–liquid flows. *AIChE J.* 23, 68–76.
- Van Rossum, J.J., 1959. Experimental investigation of horizontal liquid films. *Chem. Eng. Sci.* 11, 35.
- Wallis, G.B., 1969. One-dimensional Two-phase Flow. McGraw-Hill, Inc, New York, USA.
- Woodmansee, D.E., Hanratty, T.J., 1969. Mechanism for the removal of droplets from a liquid surface by a parallel air flow. *Chem. Eng. Sci.* 24, 299–307.
- Yun, G., Ishiwatari, Y., Ikejiri, S., Oka, Y., 2010. Numerical analysis of the onset of droplet entrainment in annular two-phase flow by hybrid method. *Ann. Nucl. Energy* 37, 230–240.
- Zhivaikin, L.Y., 1962. Liquid film thickness in film type units. *Int. Chem. Eng.* 2 (3), 337.
- Zhu, Z.F., 2004. A Study of the Interfacial Features of Gas–Liquid Annular Two-phase Flow. Ph.D. thesis. University of Saskatchewan, Saskatoon, Canada.

## Glossary

- c: wave celerity [m/s]
- $C_D$ : Drag coefficient
- $C_W$ : surface tension factor, from Ishii and Grolmes
- D: pipe diameter [m]
- DW: disturbance wave
- E: entrained fraction
- $E_0$ : Eötvös number
- f: friction factor
- $F_r$ : Froude number
- g: gravity acceleration [ $\text{m}/\text{s}^2$ ]
- $G_e$ : entrainment mass flow [ $\text{kg}/\text{m}^2 \text{s}$ ]
- $G_r$ : Grashoff number
- J: superficial velocity [m/s]
- $J^*$ : dimensionless superficial velocity
- Ku: Kutateladze number
- $L_w$ : wave spacing [m]
- $N_d$ : viscosity number
- $OE$ : onset of entrainment
- $Oh$ : Ohnesorge number
- P: wetted perimeter [m]
- $Re$ : Reynolds number
- RW: Ripples wave
- St: Strouhal number

*Stk*: Stokes number*u*: velocity [m/s]*u*<sup>\*</sup>: friction velocity [m/s]*W*: mass flow rate [kg/s]*We*: Weber number*x*: quality*X*: Lockhart–Martinelli number*Greek symbols* $\alpha$ : void fraction $\Delta h_w$ : wave amplitude or wave height [m] $\delta$ : liquid film thickness [m] $\delta_b$ : base liquid film thickness [m] $\delta^*$ : dimensionless liquid film thickness $\varphi$ : droplet diameter [m] $\lambda_w$ : wave length [m] $\mu$ : dynamic viscosity [Pa s] $\nu$ : wave frequency [Hz] $\Gamma$ : mass flow rate per unit length [kg/m s] $\Gamma^*$ : dimensionless mass flow rate per unit length $\rho$ : density [kg/m<sup>3</sup>] $\sigma$ : surface tension [N/m] $\tau$ : shear stress [Pa]*Subscripts* $\alpha$ : gas core $crit$ : critical $d$ : droplet $D$ : drag $ffOE$ : onset of entrainment $g$ : gas $i$ : interfacial $K-H$ : Kelvin–Helmholtz instability $l$ : liquid $lf$ : liquid film $le$ : entrained liquid $lfc$ : critical liquid film $max$ : maximum $min$ : minimum $R-T$ : Rayleigh–Taylor instability $w$ : wave $z$ : axial direction